Scientific Research Publishing

Journal of Applied Mathematics and Physics, 2026, 14(11), 4570-4604
https://www.scirp.org/journal/jamp
ISSN Online: 2327-4379
ISSN Print: 2327-4352

The Timeon Lattice Density and the Origin of the Critical Time Density

George Davey

Independent Researcher, West Des Moines, IA, USA
Email: George.Davey@QuantumLinear.com

How to cite this paper: Davey, G. (2026) The Timeon Lattice Density and the Origin of the Critical Time Density. *Journal of Applied Mathematics and Physics*, **14**, 4570-4604.
https://doi.org/10.4236/jamp.2026.1411225

Received: September 18, 2026
Accepted: November 16, 2026
Published: November 19, 2026

Copyright © 2026 by author(s) and Scientific Research Publishing Inc.
This work is licensed under the Creative Commons Attribution International License (CC BY 4.0).
http://creativecommons.org/licenses/by/4.0/

Open Access

Abstract

Paper 8 of this series showed that the vacuum stratum of the complex timeon field $\Phi = \hat{t}e^{i\theta}$ develops a timeon horizon where the long-wavelength phase-wave speed vanishes, and that the critical time density $\hat{t}_{\mathrm{crit}} = 2\pi/c$ is recovered only under the Spectral Lock $m_c c = 2\pi\sqrt{\kappa}\,\Omega$. This paper asks whether the Lock follows from the microscopic content of the series. It does not: the exact charged-vacuum number density $n = Z_t \kappa \hat{t}_\infty^2 \Omega / (\hbar c^2)$ converts the Lock into a primitive-cell law, $\ell^3 = 16\pi^2 \ell_{\mathrm{P}}^2 / (\sqrt{\kappa}\, m_c)$, whose coefficient Papers 1-8 leave unselected; the Baryon Partner State, dense-time saturation, and matter-Compton closures all fail to fix it. Including the rotating phase in the Pathway-B action makes the vacuum a stiff gravitational source, bounding $\sqrt{\zeta\kappa}\,\Omega$ below $4.4\times10^{-18}\ \mathrm{s}^{-1}$ today and, because the conserved charge redshifts as a^{-6}, below $7.8\times10^{-30}\ \mathrm{s}^{-1}$ at nucleosynthesis. A converged four-channel calculation of the interface shows that the transmitted flux is independent of $m_c r_s$ and is fixed by the termination of the phase channel inside the horizon: near-total reflection follows from the dense-stratum phase quench, not from the thin interface. The linear spinodal layer supplies at most 3.66 e-folds of attenuation against the 6.91 required by the no-echo bound, and the uncancelled locked vacuum lies far outside the thin-interface regime for astrophysical black holes. The critical time density is thereby reduced to a precise microscopic selection problem. All numerical results are reproduced by delivered scripts.

Keywords

Time Density, Timeon Field, Chrono-Quantum Mirror, Scalar-Tensor Gravity, Black-Hole Echoes, Spectral Lock, Charged Vacuum, Critical Time Density

1. Introduction

The time-density series has progressively replaced the original phenomenological picture of a discrete temporal substrate with field equations, phase-space structure, dense-time dynamics, and two gravitational realizations [1]-[7]. Paper 8 [8] then supplied the missing constitutive mechanism behind the Chrono-Quantum Mirror (CQM): a stationary charged vacuum carries a global phase rotation $\theta = \Omega t$, and the coupled amplitude-phase spectrum develops a finite-lapse instability where the long-wavelength phase-wave speed vanishes. The resulting timeon horizon obeys

$$N_c = \frac{\sqrt{\kappa}\Omega}{m_c c}, \quad m_c^2 \equiv \frac{V''(\hat{t}_{\text{crit}})}{Z_t}, \tag{1}$$

and the historical value $\hat{t}_{\text{crit}} = 2\pi/c$ is recovered if and only if

$$\boxed{m_c c = 2\pi\sqrt{\kappa}\Omega.} \tag{2}$$

Paper 8 therefore converted a numerical threshold into a spectral relation but deliberately left Equation (2) as a postulate.

This paper closes the next logical loop. There are two conceptually independent quantities in Equation (2): the conserved charge sector, through Ω, and the curvature of the timeon potential, through m_c. If the existing series fixes both, then the factor 2π is derived. If it does not, the missing microscopic datum should be isolated rather than hidden in a restatement of the Lock. The same exercise must also be compatible with gravity, because Paper 8's charged vacuum carries phase kinetic energy that was absent from the real-field Einstein limit of Paper 7.

The calculation leads to a sharper conclusion than a derivation of a preferred number. The Lock is not a theorem of Papers 1-8; it is a lattice-density and potential-shape selection problem. Moreover, the high-curvature reflective branch studied in Paper 8 and the uncancelled gravitationally viable charged-vacuum branch are parametrically distinct. The no-echo problem is likewise not solved by reflection alone: the spinodal layer does not supply enough demonstrated absorption. And the reflection itself, when the interface problem is solved with all channels and a well-posed outer boundary, is found to be a property of the dense-stratum phase quench rather than of the thin interface.

Because the series has developed its own vocabulary, this paper is written to be readable on its own. Section 2 summarises, without proof, the physical content of Papers 1-8 that is actually used here: the operational definition of time density, the complex timeon field and its compact $U(1)$ phase, the vacuum/atomic/dense strata, the two gravitational realisations (Pathways A and B), the critical time density $\hat{t}_{\text{crit}} = 2\pi/c$, and the constitutive meaning of the Spectral Lock. A glossary of symbols with their paper of origin is given in Table 1, and Table 2 separates the calibrations inherited from earlier papers from the inputs introduced here.

The paper is organised as follows. Section 2 is the standalone primer. Section 3

states the conventions, standing assumptions, provenance of all inherited parameters, and reconstructs the charged complex Pathway-B equations. Section 4 derives the exact number-density bridge and audits what the series actually fixes about the microscopic lattice. Section 5 tests dense-time, matter-Compton, and Planck-plus-potential closures. Section 6 derives the charged-vacuum stress and its viability region. Sections 7 and 8 solve the four-channel interface and spinodal-layer problems. Section 9 establishes the strong-field regime separation and bounds the timeon-horizon location. Section 10 collects the derived/postulated/numerical status and identifies the remaining microscopic choice. Appendix A gives the corrected BPS charge treatment and the thin-wall potential caveat required by Paper 3.

Theorem 1.1 (Paper-9 consistency theorem). Within the field content and calibrations printed in Papers 1-8, the Spectral Lock is not derived. A viable completion must additionally select the vacuum timeon density (or primitive cell volume) and the relevant potential shape. If the rotating vacuum gravitates through the minimal complex extension of Pathway B, then an uncancelled locked vacuum lies outside the high- $m_c r_s$ mirror regime; the four-channel interface transmission is fixed by the interior phase-channel termination rather than by the curvature m_c, so that reflection is a consequence of the dense-stratum phase quench and not of the thin interface; the linear spinodal layer does not by itself meet the conservative no-echo attenuation bound; and the Pathway-B timeon-horizon radius remains dependent on the global amplitude profile rather than being fixed uniquely at $1.02599 r_s$.

2. Primer: The Time-Density Framework of Papers 1-8

This section collects the definitions, postulates, and calibrations of the earlier papers that the present analysis relies on. Nothing in it is new; it is included so that the paper can be read without the preceding bibliography. Statements are attributed to the paper in which they were introduced, and the notation is that of Papers 7-8, which the present paper retains.

2.1. Time Density and the Timeon Field

Time density. The basic variable of the series is a scalar field $\hat{t}(x)$, the *time density*, defined operationally as proper time elapsed per unit proper length,

$$\hat{t} \equiv \frac{\mathrm{d}\tau}{\mathrm{d}l}, \quad \left[\hat{t}\right] = \mathrm{s}\cdot\mathrm{m}^{-1} \tag{3}$$

(Papers 2 and 3). It is a diffeomorphism scalar, in principle measurable by comparing clocks separated by a ruler. Its dimensionless form is the *temporal refractive index* $n_t \equiv c\hat{t}$; the normalisation $n_t \to 1$ in asymptotically flat space fixes the asymptotic value

$$\hat{t}_\infty = \frac{1}{c}. \tag{4}$$

The *Refractive Postulate* (Paper 3) links $\hat{t}$ to a static metric $\mathrm{d}s^2 = -N^2c^2\mathrm{d}t^2 + \cdots$ through $n_t = n_{t,\infty}/\sqrt{-g_{00}}$ (with $x^0 = ct$, so $\sqrt{-g_{00}} = N$ is the lapse), *i.e.*

$$\hat{t}(r) = \frac{\hat{t}_\infty}{N(r)}, \tag{5}$$

so that time density rises where clocks run slow. Papers 7-8 call Equation (5) the *adiabatic-tracking law*; in Section 9 it is treated as a limiting profile rather than an identity.

The timeon field. Paper 3 promotes $\hat{t}$ to the modulus of a complex scalar field, the *timeon field*,

$$\Phi(x) = \hat{t}(x)\mathrm{e}^{\mathrm{i}\theta(x)}, \ \theta \in [0, 2\pi), \tag{6}$$

whose internal phase θ carries a global, *compact* $U(1)$ symmetry $\Phi \to \mathrm{e}^{\mathrm{i}\alpha}\Phi$. The quanta of this field are called *timeons*. The field Lagrangian is scaled by a stiffness modulus Z_t so that all terms are energy densities; in the units of Papers 7-8, $[Z_t] = \mathrm{kg}\cdot\mathrm{m}^3\cdot\mathrm{s}^{-4}$. The self-interaction is a double-well potential $V(\hat{t})$ with two minima: a null-stress *vacuum* amplitude v_{vac} and a deeper, condensed *atomic* amplitude $v_{\mathrm{atom}} > v_{\mathrm{vac}}$. Paper 3 prints the representative polynomial

$$V(\hat{t}) = \lambda\left(\hat{t}^2 - v_{\mathrm{vac}}^2\right)^2\left(\hat{t}^2 - v_{\mathrm{atom}}^2\right)^2, \tag{7}$$

whose degenerate minima are discussed in Appendix A. Two curvature scales of V recur throughout: the bare asymptotic amplitude mass $m_{s,\mathrm{bare}}^2 \equiv V''(\hat{t}_\infty)/Z_t$ and the *critical curvature* $m_c^2 \equiv V''(\hat{t}_{\mathrm{crit}})/Z_t$, both with units m^{-2}; their ratio is $\xi_\infty \equiv m_c^2/m_{s,\mathrm{bare}}^2$.

Conserved charge. Because θ is compact, the $U(1)$ Noether charge of Paper 3 is the generator of 2π-periodic phase shifts and has an integer spectrum. Paper 3 writes its current as $j^\mu \propto \hat{t}^2\partial^\mu\theta$ and identifies the winding number of a localised configuration with baryon number. The canonically normalised version of this charge, and its physical unit, are stated in Definition 4.1 below; it is the quantity that this paper converts into a number density of timeons.

2.2. The Three Strata: Vacuum, Atomic, Dense

Paper 2 organises spacetime into phases of the time-density field, and Papers 5-6 give these phases a coordinate-free characterisation.

Vacuum (*regular*) *phase*. $\hat{t}$ near v_{vac}; the field supports frictionless wave propagation of both amplitude and phase perturbations. All of the gravitational and interface calculations of this paper take place in this stratum.

Atomic phase. Localised domains in which $\hat{t}$ sits at the deeper minimum v_{atom}. Paper 3 shows that such a domain, embedded in the vacuum and coupled to a matter wavefunction, forms a *Baryon Partner State* (BPS): a finite-energy, spherically symmetric configuration whose mass is the integrated gradient and potential energy of the timeon field and whose conserved charge is the $U(1)$ winding. Baryonic matter is, in this picture, confined timeons. The BPS is relevant

here only as a candidate source of charge quantisation (Section 5 and **Appendix A**).

Dense-time phase. When $\hat{t}$ exceeds the critical value $\hat{t}_{\text{crit}}$ (below), wave-supported temporal phase coherence becomes unsupported: Paper 4 shows that the interior of a black hole is a saturated state, the *Dense-Time Collective Partner State*, in which $\hat{t}$ sits on a plateau $\hat{t}_{\text{sat}}$, spatial phase gradients are quenched ($\nabla\theta \to 0$), there is no finite-frequency radiative sector, and the dynamics obey a Hamiltonian constraint rather than Schrödinger evolution. Its equation of state is stiff, $p = \varepsilon$. Papers 5-6 prove that this behaviour follows from a diverging phase-stiffness weight $\kappa(P) \to \infty$ at a threshold $P = P_\star$ of a local scalar trigger functional $P[\Phi, g]$: finite action then forces $\delta\theta = 0$ on the dense stratum, enlarging the presymplectic kernel in the phase sector and switching off the boundary central charge. The phase boundary $\mathcal{H} = \{P = P_\star\}$ is thereby characterised intrinsically. The constant κ appearing in the actions of Papers 8-9 is the finite, regular-stratum value of this stiffness weight; its absolute normalisation is not fixed by the series, which is why κ is carried explicitly in every bound below.

2.3. The Critical Time Density and the Chrono-Quantum Mirror

Paper 1 proposed that black-hole horizons are not causal boundaries but codimension-one discontinuities (*quantum mirrors*) between discrete time-density states. Paper 2 gave the threshold a value. Coherent wave transport of a field of mass m requires phase information to cross one Compton length $\lambda_C = \hbar/(mc)$ within one rest-phase period $T_0 = 2\pi\hbar/(mc^2)$; the ratio $\lambda_C/T_0 = c/(2\pi)$ is mass independent, and demanding that the local signalling speed not fall below it gives the *critical time density*

$$\hat{t}_{\text{crit}} = \frac{2\pi}{c} \simeq 2.1\times10^{-8}\,\text{s}\cdot\text{m}^{-1},\quad n_{t,\text{crit}} = 2\pi. \tag{8}$$

The surface on which $\hat{t} = \hat{t}_{\text{crit}}$ is the *Chrono-Quantum Mirror* (CQM): a finite phase boundary at which the vacuum stratum gives way to the dense stratum and radiative channels are quenched; as a surface where a wave speed in a medium vanishes, it is a horizon in the sense of analogue gravity [9] [10]. Under the tracking law (5) on a Schwarzschild exterior, $\hat{t} = \hat{t}_{\text{crit}}$ occurs where the lapse equals $N = 1/(2\pi)$, *i.e.* at

$$\frac{r_{\text{crit}}}{r_s} = \frac{1}{1-(2\pi)^{-2}} = 1.02599, \tag{9}$$

just outside the Schwarzschild radius $r_s = 2GM/c^2$. Because the CQM is reflective, Paper 2 also imposes an observational *no-echo* requirement on gravitational-wave ringdown, of the kind used to constrain exotic compact objects [11]: the round-trip amplitude coefficient must satisfy

$$G(\omega) = \sqrt{R_{\text{bar}}R_{\text{bnd}}}\,\text{e}^{-\alpha} < 10^{-3}, \tag{10}$$

where R_{bar} and R_{bnd} are the reflectivities of the outer potential barrier and of

the mirror, and α is the one-way attenuation exponent in the layer between them. With $R_{\text{bar}} = R_{\text{bnd}} = 1$ this requires $\alpha > \ln 1000 \simeq 6.91$; this is the benchmark tested in Section 8.

2.4. Two Gravitational Realisations: Pathways A and B

Paper 7 asks how $\hat{t}$ gravitates and identifies two consistent routes, both of which recover general relativity in a limit.

Pathway A (*pre-geometric calibration*). The stiffness modulus is tied to Newton's constant by the dimensionless combination

$$\zeta \equiv \frac{8\pi G Z_t \hat{t}_\infty^2}{c^4}, \quad \zeta_{\text{A}} = 1, \tag{11}$$

so that the vacuum time-density field carries exactly the Einstein-Hilbert weight.

Pathway B (*time-density-coupled gravity*, *TDCG*). The metric and $\hat{t}$ are independent fields; $\hat{t}$ couples non-minimally to curvature through $F(\hat{t})R$ with $F = (\hat{t}/\hat{t}_\infty)^2$, and ζ is a free parameter. Paper 7 shows that when $\hat{t}$ is constant at a real vacuum with $V(\hat{t}_\infty) = 0$ the field equations reduce to Einstein's and the exterior of a spherical mass is exactly Schwarzschild. Away from that limit the scalar is constrained by Solar-System post-Newtonian tests in one of two ways: either it is Yukawa-screened, which bounds the asymptotic curvature V''/Z_t from below, or it is unscreened and "stiff", which requires $\zeta \gtrsim 1.7 \times 10^5$ (the *stiff-PPN floor* used below).

The present paper works in Pathway B extended by the phase sector of Paper 8 (Assumption 3.2); Pathway A enters only as the special calibration $\zeta = 1$.

2.5. Paper 8: The Timeon Horizon and the Spectral Lock

Paper 8 supplied the constitutive mechanism behind the CQM. Its ingredients are:

1) *A charged stationary vacuum*. In a stationary, regular vacuum the timeon phase rotates uniformly, $\theta = \Omega t$, with a single conserved rate Ω fixed by the asymptotic boundary condition. This is the ground state of the compact $U(1)$ sector at fixed charge, exactly as for a Q-ball or a superfluid at fixed particle number; the vacuum is "charged" in the sense that its Noether density is nonzero.

2) *Coupled amplitude-phase spectrum*. Linearising $\Phi = (\hat{t}_0 + \delta\hat{t})\mathrm{e}^{\mathrm{i}(\Omega t + \delta\theta)}$ about a background of local lapse N gives two coupled branches: an amplitude-like (gapped) branch with local mass $M^2 = V''(\hat{t}_0)/Z_t - \kappa\Omega^2/(N^2c^2)$ and a phase-like (gapless) branch. The mixing is proportional to $\Omega\omega$. The long-wavelength phase-wave speed c_s of the gapless branch decreases as the lapse decreases.

3) *The timeon horizon*. Under the tracking law (5), c_s vanishes at a critical lapse

$$N_c = \frac{\sqrt{\kappa}\,\Omega}{m_c c}, \tag{12}$$

where M^2 changes sign. Inside this surface the amplitude branch is spinodally

unstable. Paper 8 identified this surface with the CQM and interpreted it as a reflecting interface for incoming phase waves; Section 7 revisits that identification with all four channels retained.

4) *The Spectral Lock*. The derived horizon sits at $\hat{t} = \hat{t}_{\text{crit}} = 2\pi/c$ if and only if $N_c = 1/(2\pi)$, *i.e.*

$$m_c c = 2\pi\sqrt{\kappa}\,\Omega. \tag{13}$$

Physically, the Lock states that the vacuum's phase-rotation period, $2\pi/(\sqrt{\kappa}\,\Omega)$, equals 2π light-crossing times of the critical-curvature wavelength $\lambda_c = 2\pi/m_c$; equivalently, that the rotation rate expressed in units of the critical-curvature Compton frequency $m_c c$ is exactly $1/(2\pi)$. It ties the charge sector (Ω) to the potential shape (m_c) and is the sole condition under which Paper 8 reproduces the Paper-2 value. Paper 8 states it as a postulate; the present paper asks whether it can be derived.

5) *Admissible double-well window and the sudden-interface mirror*. Paper 8 found that, under the Lock, a locked double well with $12.09 < v_{\text{atom}}/\hat{t}_\infty < 15.85$ gives an asymptotic phase speed $0.575c < c_s^\infty < c$, and computed the reflectivity of the horizon for an interface that is thin compared with the wavelength, which requires $m_c r_s \gg 10^3$. Its single-channel treatment gave a transmitted flux scaling as $(m_c r_s)^{-2/3}$; Section 7 revisits this with all four channels retained.

Table 1. Symbols used in this paper, with the paper in which each was introduced. "P9" marks quantities introduced here.

Symbol	Meaning	Origin
$\hat{t}$	time density, proper time per proper length (s·m^{-1})	P2, P3
$n_t = c\hat{t}$	temporal refractive index	P2
$\hat{t}_\infty = 1/c$	asymptotic (flat-space) time density	P2, P7
$\hat{t}_{\text{crit}} = 2\pi/c$	critical time density; CQM location	P2
$\Phi = \hat{t}e^{i\theta}$	complex timeon field; compact $U(1)$ phase θ	P3
Z_t	stiffness modulus (kg·m^3·s^{-4})	P3, P7
$V(\hat{t})$, v_{vac}, v_{atom}	double-well potential and its vacuum/atomic minima	P3
κ	phase-stiffness weight (regular-stratum value)	P5-P6, P8
N	lapse, $\sqrt{-g_{00}}$ with $x^0 = ct$; $N^2 = 1 - r_s/r$ on Schwarzschild	P7
$F = (\hat{t}/\hat{t}_\infty)^2$	non-minimal curvature coupling (Pathway B)	P7
$\zeta = 8\pi G Z_t \hat{t}_\infty^2/c^4$	gravitational weight of the vacuum field; $\zeta = 1$ in Pathway A	P7
Ω	global phase-rotation rate of the charged vacuum (rad·s^{-1})	P8
$m_c^2 = V''(\hat{t}_{\text{crit}})/Z_t$	critical curvature (m^{-2})	P8
$m_{s,\text{bare}}^2 = V''(\hat{t}_\infty)/Z_t$	bare asymptotic curvature	P7, P8
$\xi_\infty = m_c^2/m_{s,\text{bare}}^2$	curvature ratio	P8
$N_c = \sqrt{\kappa}\,\Omega/(m_c c)$	critical lapse (timeon horizon)	P8
c_s, c_s^∞	long-wavelength phase-wave speed; asymptotic value	P8

Continued

$\mathcal{R} = m_c c \big/ \left(\sqrt{\kappa}\Omega\right)$	spectral ratio; Lock $\Leftrightarrow \mathcal{R} = 2\pi$	P8, P9
R_{bar}, R_{bnd}, α	barrier/mirror reflectivities, attenuation exponent	P2
n, ℓ	timeon number density, primitive cell length	P9
K_θ, ε_{vac}, p_{vac}	phase kinetic density; vacuum energy density and pressure	P9
ρ_Λ	benchmark dark-energy density, 5.3×10^{-10} J·m^{-3}	P9
ϵ_{red}	validity parameter of the reduced radial model	P9

3. Framework, Conventions, Provenance, and Standing Assumptions

We retain the Paper-7/Paper-8 convention

$$\left[\hat{t}\right] = \text{s}\cdot\text{m}^{-1},\ \left[Z_t\right] = \text{kg}\cdot\text{m}^3\cdot\text{s}^{-4},\ \left[m_c\right] = \left[m_s\right] = \text{m}^{-1},\ \hat{t}_\infty = 1/c, \tag{14}$$

and write $\Phi = \hat{t}\text{e}^{\text{i}\theta}$.

3.1. Metric, Time-Coordinate, and Phase Conventions

The following conventions are used in every stress-tensor and stationary-phase statement below.

Signature and coordinates. The metric signature is $(-,+,+,+)$ with coordinates $x^\mu = (ct, \boldsymbol{x})$, so that $(\nabla\theta)^2 \equiv g^{\mu\nu}\partial_\mu\theta\partial_\nu\theta = -\dot{\theta}^2/c^2 + |\nabla\theta|^2$ in flat space, and similarly for $(\nabla\hat{t})^2$. For a static spherically symmetric background we write $\text{d}s^2 = -N^2c^2\text{d}t^2 + N^{-2}\text{d}r^2 + r^2\text{d}\Omega^2$, with $N^2 = 1 - r_s/r$ on Schwarzschild; the coefficients $a = \left(N^2c^2\right)^{-1}$ and $b = N^2$ appearing in Sections 7-8 are $-g^{00}/c^2$ and g^{rr} respectively (with $x^0 = ct$, $g_{00} = -N^2$ and $g^{00} = -N^{-2}$; we write g_{00} rather than g_{tt} throughout, so that g_{tt} in the coordinate-time sense would be $c^2 g_{00}$). $G_{\mu\nu}$ and $T_{\mu\nu}$ are defined so that $T_{\mu\nu} = -\dfrac{2}{\sqrt{-g}}\dfrac{\delta\left(\sqrt{-g}\mathcal{L}_\Phi\right)}{\delta g^{\mu\nu}}$, giving Equation (23).

Time coordinate. t is the asymptotic Killing time, *i.e.* the proper time of a static observer at spatial infinity where $N = 1$ and $\hat{t} = \hat{t}_\infty$. A static observer at lapse N measures proper time $\text{d}\tau = N\text{d}t$.

Stationary phase. The charged vacuum is $\theta = \Omega t + \theta_0$ with Ω constant; θ is dimensionless and 2π-periodic, so Ω is in rad s^{-1} and is the rotation rate as measured by the asymptotic clock. The locally measured rate at lapse N is Ω/N, which is why the local combination $\kappa a\Omega^2 = \kappa\Omega^2/\left(N^2c^2\right)$ appears in M^2. Phase perturbations are written $\delta\theta$ with no rescaling; the rescaled variables $\chi = \sqrt{\kappa}\hat{t}_\infty\delta\theta$ and $q_\theta = \sqrt{\kappa}\hat{t}_0\delta\theta$ are introduced only to make the perturbation matrices Hermitian.

Energy density and pressure. For the homogeneous rotating vacuum ($\hat{t} = \hat{t}_\infty$, $\nabla\hat{t} = \nabla\theta = 0$, $g_{\mu\nu} = \eta_{\mu\nu}$), $\partial_0\theta = \Omega/c$ and $(\nabla\theta)^2 = -\Omega^2/c^2$, so Equation (23)

gives

$$\varepsilon_{\text{vac}} \equiv T_{00}^{(\Phi)} = Z_t \kappa \hat{t}_\infty^2 \frac{\Omega^2}{c^2} + \left[-\frac{Z_t}{2} \kappa \hat{t}_\infty^2 \frac{\Omega^2}{c^2} + V \right] = K_\theta + V\left(\hat{t}_\infty\right), \tag{15}$$

$$p_{\text{vac}} \delta_{ij} \equiv T_{ij}^{(\Phi)} = -\delta_{ij} \left[-\frac{Z_t}{2} \kappa \hat{t}_\infty^2 \frac{\Omega^2}{c^2} + V \right] = \left(K_\theta - V\left(\hat{t}_\infty\right) \right) \delta_{ij}, \tag{16}$$

with $K_\theta = \frac{1}{2} Z_t \kappa \hat{t}_\infty^2 \Omega^2 / c^2$. These are the expressions quoted in Equation (44); the check that $\left[Z_t \kappa \hat{t}_\infty^2 \Omega^2 / c^2 \right] = \text{kg} \cdot \text{m}^3 \cdot \text{s}^{-4} \cdot \text{s}^2 \cdot \text{m}^{-2} \cdot \text{s}^{-2} \cdot \text{s}^2 \cdot \text{m}^{-2} = \text{J} \cdot \text{m}^{-3}$ confirms the unit convention. The canonical momentum conjugate to θ that follows from the same conventions is $\pi_\theta = \partial \mathcal{L} / \partial \dot{\theta} = Z_t \kappa \hat{t}^2 \dot{\theta} / c^2$, which is used in Definition 4.1.

3.2. Provenance of Parameters and Boundary Conditions

Table 2 and Table 3 list every numerical or structural input used in this paper and state whether it is inherited from Papers 1-8 or introduced here, so that each claimed consequence can be traced to its calibration assumptions.

Table 2. Provenance of inputs (field content, units, and calibrations; boundary conditions in Table 3). "Inherited" entries are taken from the cited paper without modification; "P9" entries are choices made in this paper and are not results of the series.

Input	Value/form	Status and source
Field content and units		
Units $\left[\hat{t}\right] = \text{s} \cdot \text{m}^{-1}$, $\left[Z_t\right] = \text{kg} \cdot \text{m}^3 \cdot \text{s}^{-4}$, $\left[m_c\right] = \left[m_s\right] = \text{m}^{-1}$	—	Inherited (P7, P8)
Asymptotic amplitude	$\hat{t}_\infty = 1/c$	Inherited (P2 normalisation $n_t \to 1$; P7)
Compact global $U(1)$, $\theta \in [0, 2\pi)$	—	Inherited (P3)
Double-well form	$\lambda\left(\hat{t}^2 - v_{\text{vac}}^2\right)^2 \left(\hat{t}^2 - v_{\text{atom}}^2\right)^2$	Inherited (P3); degeneracy noted in App. A
Phase-stiffness weight κ	free, $\kappa > 0$	Inherited structure (P5-P6, P8); normalisation not fixed by the series
Non-minimal coupling	$F = \left(\hat{t}/\hat{t}_\infty\right)^2$	Inherited (P7, Pathway B)
Phase kinetic term $\frac{Z_t}{2} \kappa \hat{t}^2 (\nabla\theta)^2$ in the Pathway-B action	Equation (17)	**P9** (Assumption 3.2); same term as P8 but P8 did not couple it to gravity
Calibrations		
Pathway-A weight	$\zeta = 1$	Inherited (P7A)
Stiff-PPN floor	$\zeta \gtrsim 1.7 \times 10^5$	Inherited (P7B)
Critical time density	$\hat{t}_{\text{crit}} = 2\pi/c$	Inherited (P2)
Critical lapse	$N_c = \sqrt{\kappa}\Omega / (m_c c)$	Inherited (P8)
Spectral Lock	$m_c c = 2\pi\sqrt{\kappa}\Omega$	Inherited as a *postulate* (P8); tested here, not assumed except where stated
Admissible locked window	$12.09 < v_{\text{atom}} / \hat{t}_\infty < 15.85$	Inherited (P8)

Continued

Illustrative double well for scans	$v_{\text{atom}}/v_{\text{vac}} = 13$ (and 20, 30, 100, 400)	**P9**; 13 lies inside the P8 window
Dense/vacuum density ratio	$R = 50$	Inherited, illustrative only (P2); not used in any bound
No-echo requirement	$G < 10^{-3}$, $R_{\text{bar}} = R_{\text{bnd}} = 1$	Inherited (P2); unit reflectivities are the conservative P9 choice
Benchmark dark-energy density	$\rho_\Lambda = 5.3 \times 10^{-10}\ \text{J}\cdot\text{m}^{-3}$	**P9** (Assumption 3.3); standard present-day value
Radiation density today, BBN temperature, g_*, g_{*_s}	$\rho_{r,0} = 7.06 \times 10^{-14}\ \text{J}\cdot\text{m}^{-3}$, $T_{\text{BBN}} = 1\,\text{MeV}$, $g_* = g_{*_s} = 10.75$, $g_{*_s,0} = 3.91$, $a_{\text{BBN}} = 1.68 \times 10^{-10}$	**P9** (Section 6.1); standard cosmology [12] [13]
BPS benchmark	$R = 1\,\text{fm}$, $\Delta N = 1$, $\left(v_{\text{atom}}/\hat{t}_\infty\right)^2 - 1 = 168$	**P9**; illustrative, Section 5
Matter-Compton masses	m_e, m_p	**P9**; illustrative
Interface frequencies and curvatures	$\omega r_s/c \in \{1,3\}$, $m_c r_s \in \left[10^4, 10^6\right]$	**P9**

Table 3. Provenance of inputs, continued: boundary conditions.

Input	Value/form	Status and source
	Boundary conditions	
Vacuum at infinity	$\hat{t} \to \hat{t}_\infty$, $N \to 1$	Inherited (P7)
Stationary phase at infinity	$\theta \to \Omega t$, single global Ω	Inherited (P8)
Amplitude profile on the exterior	tracking $\hat{t} = \hat{t}_\infty/N$	Inherited (P3 Refractive Postulate, P8); used here as a diagnostic limit, not assumed to be a Pathway-B solution
BPS regularity	$\hat{t}$ finite, θ single-valued at $r \to 0$	Inherited (P3); consequence $Q = 0$ derived in App. A
Scattering boundary conditions	open channel carried to $R_{\text{far}} = 100 r_s$ with WKB data; outward-decaying outer partner; inward amplitude wave inside; inner phase partner terminated by (E) decaying seed, (Q) dense-stratum quench $\delta\theta = 0$, or (N) Neumann, at a stated radius	**P9** (Section 7.2); (Q) inherits the phase quench of P4-P6
FRW phase evolution	$\text{d}\left(a^3 \kappa \hat{t}^2 \dot{\theta}\right)/\text{d}t = 0$	Derived here from Equation (25)

Assumption 3.1 (Charged stationary vacuum). In a stationary regular vacuum with no superflow the phase is $\theta = \Omega t$, with one conserved rate Ω fixed at infinity, as in Paper 8. Its magnitude is not assumed to be fixed a priori.

Assumption 3.2 (Minimal complex Pathway-B completion). Paper 7's Pathway-B action is extended by the same $U(1)$ phase kinetic term used in Paper 8, without adding an independent stress-cancellation sector:

$$S=\int \mathrm{d}^4x\sqrt{-g}\left[\frac{c^4}{16\pi G}F\left(\hat{t}\right)R-\frac{Z_t}{2}\left(\left(\nabla\hat{t}\right)^2+\kappa\hat{t}^2\left(\nabla\theta\right)^2\right)-V\left(\hat{t}\right)+\mathcal{L}_m\right], \tag{17}$$

with $F=\left(\hat{t}/\hat{t}_\infty\right)^2$.

Assumption 3.3 (No-cancellation benchmark). When testing whether the written charged vacuum is gravitationally viable without additional dynamics, its homogeneous phase stress is required not to exceed the benchmark dark-energy density $\rho_\Lambda=5.3\times10^{-10}\,\mathrm{J\cdot m^{-3}}$. This is a present-background benchmark: it is evaluated at scale factor $a=1$ with the present asymptotic amplitude $\hat{t}_\infty=1/c$, and it is a necessary condition only. Its relation to the cosmological evolution of the conserved phase charge is worked out in Section 6.1.

Assumption 3.4 (Reduced radial interface model). For the interface calculation we promote the local Paper-8 WKB amplitude-phase matrix to a radial second-order system and neglect derivatives of the local eigenvector normalisation and other background-gradient terms, matching the approximation used by Paper 8's single-channel appendix. Conclusions about the curvature dependence of the transmission are therefore conditional on this reduced radial model. The neglected terms are all first-derivative terms proportional to the logarithmic gradient of the background: the normalisation of the phase variable $q_\theta=\sqrt{\kappa}\hat{t}_0\delta\theta$ carries $\hat{t}_0'/\hat{t}_0=-N'/N$, and the radial coefficients $a=\left(N^2c^2\right)^{-1}$, $b=N^2$ carry $\pm2N'/N$. Relative to the retained second-derivative terms they are of order

$$\boxed{\epsilon_{\mathrm{red}}\left(r\right)\equiv\frac{\left|\mathrm{d}\ln N/\mathrm{d}r\right|}{k_{\mathrm{loc}}\left(r\right)},} \tag{18}$$

where k_{loc} is the smallest local channel wavenumber at r, taken as $\left|\mathrm{Re}\,k\right|$ for an open channel and $\left|\mathrm{Im}\,k\right|$ for an evanescent one. The reduced model is valid where $\epsilon_{\mathrm{red}}\ll1$ throughout the region that controls the quantity of interest. For the curvature dependence of the transmission, the controlling region is the nonadiabatic conversion layer at the timeon horizon, where $M^2\sim S$ and all four channel wavenumbers are of order $k_{\mathrm{loc}}\simeq\sqrt{S}/N$ with $S=4\sqrt{\kappa}a\Omega\omega$. Under the Lock, $S=2m_c\omega/\left(\pi N^2c\right)$, and on a Schwarzschild exterior at the horizon lapse $N=1/\left(2\pi\right)$ one has $\left|\mathrm{d}\ln N/\mathrm{d}r\right|\simeq2\pi^2/r_s$, so that

$$\boxed{\epsilon_{\mathrm{red}}^{\mathrm{layer}}\simeq\frac{1}{2}\sqrt{\frac{\pi}{2}}\left[\left(m_cr_s\right)\left(\omega r_s/c\right)\right]^{-1/2}=0.627\left[\left(m_cr_s\right)\left(\omega r_s/c\right)\right]^{-1/2}.} \tag{19}$$

We adopt $\epsilon_{\mathrm{red}}^{\mathrm{layer}}\le10^{-2}$ as the criterion for reading the four-channel interface results as reliable within the reduced radial model; it defines the parameter region

$$\boxed{\left(m_cr_s\right)\left(\omega r_s/c\right)\gtrsim4\times10^3.} \tag{20}$$

Every four-channel run reported in Section 7 lies inside it ($\epsilon_{\mathrm{red}}^{\mathrm{layer}}$ runs from 6.3×10^{-3} at $m_cr_s=10^4$ to 6.3×10^{-4} at 10^6), and the criterion coincides with Paper 8's thin-interface requirement $m_cr_s\gg10^3$. Outside the layer, in the outer phase-dominated region, the open-channel wavenumber is

$$k \simeq \frac{\omega}{N^2 c}, \text{ so that } \epsilon_{\mathrm{red}}^{\mathrm{outer}} \simeq \frac{1}{2}\left(\frac{\omega r_s}{c}\right)^{-1}\left(\frac{r_s}{r}\right)^2, \tag{21}$$

the N^{-2} factors of $\left|\mathrm{d}\ln N/\mathrm{d}r\right| = r_s/\left(2r^2N^2\right)$ and of k cancelling. This quantity is independent of m_c and therefore cannot generate an m_c-dependence or alter the conclusion that fixed-radius terminations give curvature-independent transmission. At $\omega r_s/c = 1$, however, $\epsilon_{\mathrm{red}}^{\mathrm{outer}}$ reaches approximately 0.47 near r_c, so the absolute transmission coefficients of the reduced radial model are not controlled at the ten-percent level there and may carry order-unity systematic uncertainty until the fully covariant spherical perturbation equation is solved. The parameter decreases as $\left(\omega r_s/c\right)^{-1}$ and as $\left(r_s/r\right)^2$ away from the horizon. The eigenvector-rotation terms inside the conversion layer are not neglected: the coupled 2×2 system (61) is integrated without a local diagonalisation, so mode conversion is computed rather than approximated.

Assumption 3.5 (Spinodal attenuation proxy). For an upper-envelope test of transition-layer absorption, each e-fold of the fastest linear spinodal instability is counted as one e-fold of irreversible attenuation. This deliberately favours the hypothesis that the layer absorbs; the underlying linear field equations are conservative and do not by themselves produce entropy.

Variation of Equation (17) gives

$$FG_{\mu\nu} = \frac{8\pi G}{c^4}\left(T_{\mu\nu}^{(m)} + T_{\mu\nu}^{(\Phi)}\right) + \left(\nabla_\mu\nabla_\nu - g_{\mu\nu}\Box\right)F, \tag{22}$$

$$\begin{aligned} T_{\mu\nu}^{(\Phi)} &= Z_t\partial_\mu\hat{t}\,\partial_\nu\hat{t} + Z_t\kappa\hat{t}^2\partial_\mu\theta\,\partial_\nu\theta \\ &\quad - g_{\mu\nu}\left[\frac{Z_t}{2}\left(\left(\nabla\hat{t}\right)^2 + \kappa\hat{t}^2\left(\nabla\theta\right)^2\right) + V\left(\hat{t}\right)\right], \end{aligned} \tag{23}$$

$$Z_t\left[\Box\hat{t} - \kappa\hat{t}\left(\nabla\theta\right)^2\right] - V'\left(\hat{t}\right) = -\frac{c^4}{16\pi G}F'\left(\hat{t}\right)R, \tag{24}$$

$$\nabla_\mu\left(\kappa\hat{t}^2\nabla^\mu\theta\right) = 0. \tag{25}$$

These equations reduce to Paper 7's real-amplitude TDCG equations when the phase is constant.

4. The Microscopic Lattice-Density Problem

4.1. What the Series Fixes and What It Does Not

The microscopic number density and cell length have units $[n] = \mathrm{m}^{-3}$ and $[\ell] = \mathrm{m}$, whereas $\hat{t}$ is an operational clock-density amplitude. Consequently neither $\hat{t}$ nor Paper 4's $\hat{t}_{\mathrm{sat}}$ can be identified dimensionally with a three-density or cell volume. Table 4 lists what each earlier paper commits to about the lattice and what follows from it.

Paper 4 therefore cannot close the problem by itself. Even if an occupancy map were postulated,

$$\frac{n\left(\hat{t}\right)}{n_\infty} = f\left(\frac{\hat{t}}{\hat{t}_\infty}\right), \quad f\left(1\right) = 1, \tag{26}$$

no such f and no numerical $\hat{t}_{\mathrm{sat}}$ are specified. Moreover, the charged-vacuum number density derived below belongs to the rotating regular phase, while the dense phase suppresses temporal phase variation.

Table 4. Lattice commitments of the series relevant to Paper 9. The final column states what follows without an additional constitutive identification.

Source	Commitment	Consequence for n or ℓ
Paper 2	Discrete timeons; fundamental lattice; illustrative dense/vacuum temporal-density ratio $R=50$.	No absolute cell spacing or number-density normalisation.
Paper 3	Double-well vacuum/atomic amplitudes and a global $U(1)$ symmetry.	The static radial constant is not a temporal charge; no vacuum Ω is selected.
Paper 4	Dense phase saturates at $\hat{t}_{\mathrm{sat}}$ and suppresses phase motion.	Saturation is an amplitude plateau, not a regular-vacuum Noether-density maximum.
Paper 7A	$\zeta = 8\pi G Z_t \hat{t}_\infty^2 / c^4 = 1$ in the pre-geometric calibration.	Converts a chosen Ω into n but does not choose either.
Paper 7B	ζ is free; scalar screening constrains V''/Z_t.	Constrains curvature, not primitive cell volume.
Paper 8	Stationary charged vacuum has global Ω; the Lock selects one charge sector.	Supplies the density bridge once n or ℓ is independently specified.

4.2. Exact Number-Density Bridge

Before converting the canonical charge into a particle density we state the two facts that make the conversion normalisation independent.

Definition 4.1 (Compact $U(1)$ and the unit of timeon charge). 1) The $U(1)$ of the timeon field is compact: θ is defined modulo 2π, as in Paper 3, so field configurations differing by $\theta \to \theta + 2\pi$ are identical and the phase may carry integer winding. 2) With the conventions of Section 3.1, the canonical momentum density conjugate to θ obtained from Equation (17) is

$$\pi_\theta = \frac{\partial \mathcal{L}}{\partial \dot{\theta}} = \frac{Z_t \kappa \hat{t}^2 \dot{\theta}}{c^2}, \quad [\pi_\theta] = \mathrm{J \cdot s \cdot m^{-3}}, \tag{27}$$

and the Noether charge of the global phase shift is $\mathcal{Q} = \int \pi_\theta \mathrm{d}^3 x$, with units of action. Because θ is compact, $\mathcal{Q}$ generates a $U(1)$ rather than an $\mathbb{R}$, and its canonically quantised spectrum is $\mathcal{Q} = \hbar \mathcal{N}$ with $\mathcal{N} \in \mathbb{Z}$; equivalently, the wave functional must be single valued under $\theta \to \theta + 2\pi$. The *unit of timeon charge* is therefore one quantum $\hbar$ of phase action, and a *timeon* in the sense used below is one quantum of $\mathcal{N}$. The timeon number density is

$$n \equiv \frac{\pi_\theta}{\hbar} = \frac{Z_t \kappa \hat{t}^2 \dot{\theta}}{\hbar c^2}, \quad [n] = \mathrm{m^{-3}}. \tag{28}$$

Remark 4.1. Two comments delimit this definition. First, if the $U(1)$ were non-compact ($\theta \in \mathbb{R}$), $\mathcal{Q}$ would be a continuous real parameter, $\hbar$ would enter only as an arbitrary unit, and "one timeon per primitive cell" would have no

invariant meaning; the compactness inherited from Paper 3 is what makes n a particle density. Second, Paper 3 writes the current with the convention-free normalisation $j^{\mu} \propto \hat{t}^2 \partial^{\mu}\theta$ and quotes only the dimensionless winding number of a BPS; Equation (28) is the same current multiplied by the fixed factor $Z_t \kappa / \left(\hbar c^2\right)$ that follows from the action, so the two are proportional and no additional constant is available to rescale n. The occupancy identification $n = \ell^{-3}$ made below is then the single remaining convention: it defines the primitive cell as the volume containing one quantum of $\mathcal{N}$.

For a homogeneous charged vacuum, setting $\hat{t} = \hat{t}_{\infty}$ and $\dot{\theta} = \Omega$ in Equation (28), the canonical temporal $U(1)$ charge gives

$$\boxed{n = \frac{Z_t \kappa \hat{t}_{\infty}^2 \Omega}{\hbar c^2}.} \tag{29}$$

Defining, as in Paper 7,

$$\zeta \equiv \frac{8\pi G Z_t \hat{t}_{\infty}^2}{c^4}, \quad \ell_{\mathrm{P}}^2 = \frac{\hbar G}{c^3}, \tag{30}$$

Equation (29) becomes

$$\boxed{n = \frac{\zeta \kappa \Omega}{8\pi c \ell_{\mathrm{P}}^2}.} \tag{31}$$

If one timeon occupies one primitive cell, $n = \ell^{-3}$, then

$$\boxed{\ell^3 = \frac{8\pi c \ell_{\mathrm{P}}^2}{\zeta \kappa \Omega}.} \tag{32}$$

This relation is exact under the stated charge normalisation, but it is not a vacuum-selection equation.

Theorem 4.1 (Lattice-density underdetermination). Papers 1-8 do not determine the homogeneous vacuum cell volume ℓ^3 or, equivalently, the conserved charge sector Ω.

Proof. Papers 1-6 provide no independent three-density normalisation. Paper 7 fixes only the conversion factor between Ω and n through ζ; Pathway B leaves ζ itself free. Paper 4's saturation amplitude is not a temporal Noether density. Paper 8 proves that Ω is spatially global in a stationary vacuum but leaves its magnitude as a conserved-state parameter. Equation (32) is therefore a one-parameter family rather than a prediction.

4.3. The Lock as a Cell-Volume Statement

If the only dimensional microscopic ingredients in the primitive volume are one Planck area and the critical curvature length, the general one-scale monomial is

$$\ell^3 = C \frac{\ell_{\mathrm{P}}^2}{\sqrt{\kappa} m_c}, \tag{33}$$

with dimensionless coefficient C. Combining with Equation (32) gives

$$\boxed{\mathcal{R} \equiv \frac{m_c c}{\sqrt{\kappa}\Omega} = \frac{C\zeta}{8\pi}.} \tag{34}$$

For the Pathway-A calibration $\zeta = 1$, the Spectral Lock is exactly $C = 16\pi^2$, or equivalently

$$\boxed{n = \frac{\sqrt{\kappa} m_c}{16\pi^2 \ell_{\mathrm{P}}^2},\ \ell^3 = \frac{16\pi^2 \ell_{\mathrm{P}}^2}{\sqrt{\kappa} m_c} = \frac{8\pi \ell_{\mathrm{P}}^2 \lambda_c}{\sqrt{\kappa}},\ \lambda_c = \frac{2\pi}{m_c}.} \tag{35}$$

Thus, the earlier $2\pi/c$ value is equivalent to a microscopic density law. Equation (35) identifies the missing input but does not derive it; Figure 1 shows the single-scale closure and the unselected locked value of C.

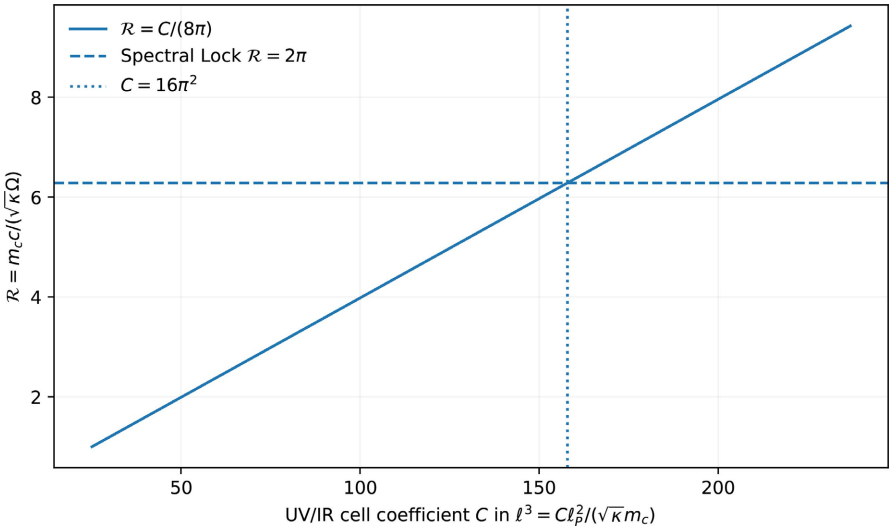


Figure 1. Single-scale lattice closure in the Pathway-A normalisation. Dimensional analysis reduces the unknown microscopic law to a dimensionless coefficient C, but the Spectral Lock corresponds to the specific unselected value $C = 16\pi^2$.

5. Tests of Natural Microscopic Closures

5.1. Dense-Time Saturation

Identifying $\hat{t}_{\mathrm{sat}}$ with a maximum cell occupancy fails both dimensionally and dynamically. It would require an additional constitutive map $n(\hat{t})$ and an absolute normalisation. Further, Paper 4 suppresses temporal phase rotation in the saturated phase, whereas Equation (29) applies to the rotating regular vacuum. Dense-time saturation therefore does not fix Ω or ℓ.

5.2. Matter-Compton Closure

A second possibility is

$$\Omega = \frac{mc^2}{\hbar} \tag{36}$$

for some matter mass m. Equation (32) then gives

$$\ell = \left(\frac{8\pi \ell_{\mathrm{P}}^2 \bar{\lambda}_C}{\zeta \kappa} \right)^{1/3}, \quad \bar{\lambda}_C = \frac{\hbar}{mc}. \tag{37}$$

For $\zeta = \kappa = 1$, the electron gives $\ell = 1.3636 \times 10^{-27}$ m and, if the Lock is separately imposed, $m_c = 1.6271 \times 10^{13}\ \mathrm{m}^{-1}$. The proton gives $\ell = 1.1135 \times 10^{-28}$ m and $m_c = 2.9876 \times 10^{16}\ \mathrm{m}^{-1}$. Both easily satisfy microscopic Yukawa screening if the Lock is separately supplied.

The series, however, singles out no matter mass as the vacuum clock. Paper 2's coherence estimate is mass-independent after taking the ratio of Compton length and rest-phase period; Paper 3's proton target concerns a localised BPS, not the homogeneous vacuum; and Paper 8's electron value is an illustrative microscopic scale. Equation (36) is therefore a family of hypotheses rather than a prediction.

5.3. BPS Excess Charge and the Hubble-Scale Coincidence

A charged stationary BPS is Q-ball-like, $\Phi = \hat{t}(r) \mathrm{e}^{\mathrm{i}\Omega t}$, and rotates at the vacuum's already-selected Ω. Its excess charge is approximately

$$\Delta N \simeq n \left[\left(\frac{v_{\mathrm{atom}}}{\hat{t}_\infty} \right)^2 - 1 \right] \frac{4\pi R^3}{3}. \tag{38}$$

Setting $\Delta N = 1$, $R = 1$ fm, and the representative enhancement factor $\left[\left(v_{\mathrm{atom}} / \hat{t}_\infty \right)^2 - 1 \right] = 168$ gives

$$\Omega = 2.797 \times 10^{-18}\ \mathrm{s}^{-1}, \tag{39}$$

which is numerically close to the Hubble rate. This is an interesting dimensional coincidence, but it does not select the vacuum: changing the assumed BPS radius changes the inferred value, and the BPS charge is determined by the background Ω and its size rather than the reverse.

5.4. Planck Scale Plus Potential Parameters

A horizon-free candidate can be written using the asymptotic amplitude curvature $m_{s,\mathrm{bare}}$ rather than m_c.

Postulate 5.1 (Asymptotic Lattice-Density Postulate—tested candidate). One conserved timeon occupies a primitive regular-vacuum cell of volume

$$\ell^3 = \frac{A_G \lambda_s}{\sqrt{\kappa}}, \quad A_G \equiv \frac{4Gh}{c^3} = 8\pi \ell_{\mathrm{P}}^2, \quad \lambda_s = \frac{2\pi}{m_{s,\mathrm{bare}}}. \tag{40}$$

This candidate mentions neither a black-hole horizon nor the target factor in Equation (2). In Pathway A it predicts

$$\Omega = \frac{m_{s,\mathrm{bare}} c}{2\pi \sqrt{\kappa}}, \quad \mathcal{R} = 2\pi \frac{m_c}{m_{s,\mathrm{bare}}} = 2\pi \sqrt{\xi_\infty}, \tag{41}$$

where $\xi_\infty \equiv m_c^2 / m_{s,\mathrm{bare}}^2$. The Spectral Lock then requires the separate condition $\xi_\infty = 1$.

For the actual double well the crossing occurs numerically at

$$\frac{v_{\text{atom}}}{v_{\text{vac}}} = 12.58613, \quad \frac{v_{\text{atom}}}{\hat{t}_\infty} = 12.25502, \quad \xi_\infty = 1, \tag{42}$$

inside Paper 8's admissible window. But Equation (40) does not select this potential shape. For example, $v_{\text{atom}}/v_{\text{vac}} = 13$ gives $\mathcal{R} = 6.4870$, not 2π.

Theorem 5.1 (No non-circular one-input derivation). No closure already fixed by Papers 1-8 has been found that determines the primitive lattice density and simultaneously forces the Spectral Lock. Dense-time saturation does not define n; a matter-Compton closure contains an unselected mass; and the strongest tested horizon-free Planck-plus-potential closure still leaves one independent potential-shape parameter.

If the microscopic coefficient differs from the locked value, the critical radius and the admissible double-well window move. For example, taking $\mathcal{R} = \pi$ gives numerically

$$5.9104 < \frac{v_{\text{atom}}}{\hat{t}_\infty} < 7.8384, \quad 0.5674c < c_s^\infty < c, \quad r_{\text{crit}} = 1.1127 r_s \tag{43}$$

on a Schwarzschild/Refractive exterior, whereas $\mathcal{R} = 2\pi$ gives the Paper-8 window $12.0932 < v_{\text{atom}}/\hat{t}_\infty < 15.8478$, $0.5750c < c_s^\infty < c$, and $r_{\text{crit}} = 1.0260 r_s$. The number 2π therefore cannot be absorbed harmlessly into a convention.

6. The Charged Vacuum as a Gravitational Source

Theorem 6.1 (Charged-vacuum gravitation). Under Assumption 3.2, Paper 8's rotating vacuum is a gravitational source in Pathway B. Paper 7's vanishing-vacuum-stress Einstein limit is recovered only when $\Omega = 0$ together with $V(\hat{t}_\infty) = 0$, or when additional dynamics cancel the complete phase stress tensor.

Proof. For a locally homogeneous background $\hat{t} = \hat{t}_\infty$, $\theta = \Omega t$, Equation (23) is a perfect-fluid stress tensor with

$$\boxed{K_\theta = \frac{1}{2} Z_t \kappa \hat{t}_\infty^2 \frac{\Omega^2}{c^2}, \quad \varepsilon_{\text{vac}} = K_\theta + V(\hat{t}_\infty), \quad p_{\text{vac}} = K_\theta - V(\hat{t}_\infty).} \tag{44}$$

Thus $\Omega \neq 0$ contributes positive energy even when the amplitude is spatially constant.

The kinetic phase component has $p_\theta = \varepsilon_\theta$. In a spatially flat FRW background, Equation (25) gives

$$\frac{\mathrm{d}}{\mathrm{d}t}\left(a^3 \kappa \hat{t}^2 \dot{\theta}\right) = 0, \tag{45}$$

so for nearly fixed amplitude $\dot{\theta} \propto a^{-3}$ and $K_\theta \propto a^{-6}$. The rotating phase is therefore a stiff component, not a cosmological constant. Numerical locked double-well solutions with the zero-offset potential have positive p/ε, approaching approximately 1/3 at large $v_{\text{atom}}/v_{\text{vac}}$ rather than −1.

6.1. Cosmological Applicability of the Viability Gate

Assumption 3.3 is applied at the present epoch. The stiff redshifting just derived

determines how far that benchmark can be extrapolated, and the answer delimits the gate sharply.

Charge conservation fixes the history. The conserved comoving charge is $a^3 n$ with n given by Equation (28). If the asymptotic amplitude and the stiffness weight are cosmologically constant, $\hat{t}_\infty = 1/c$ and $\kappa = \text{const}$ (the minimal reading of Papers 7-8, in which $\hat{t}_\infty$ is a fixed normalisation rather than a dynamical cosmological field), then

$$\Omega(a) = \Omega_0 a^{-3}, \; K_\theta(a) = K_\theta^{(0)} a^{-6}, \tag{46}$$

where the subscript 0 denotes present values. A charged vacuum that satisfies Equation (51) today therefore carried a larger phase stress at every earlier epoch, growing faster than radiation (a^{-4}) and matter (a^{-3}).

The present gate is necessary, not sufficient. Suppose the gate were saturated today, $K_\theta^{(0)} = \rho_\Lambda$. With the present matter density $\rho_{m,0} \simeq 2.4 \times 10^{-10}\ \mathrm{J \cdot m^{-3}}$, the stiff component would have exceeded matter for all $a < \left(\rho_\Lambda / \rho_{m,0}\right)^{1/3} \simeq 1.3$, *i.e.* throughout cosmic history, and would have exceeded radiation ($\rho_{r,0} = 7.06 \times 10^{-14}\ \mathrm{J \cdot m^{-3}}$ for photons and three neutrino species) at all $a < 86$. Such a history is excluded by the observed matter- and radiation-dominated eras. Compliance with Assumption 3.3 at $a = 1$ is thus a necessary condition for the rotating solution, but it does not establish compatibility with the cosmological evolution of the conserved charge.

A nucleosynthesis-era condition. A sufficient benchmark within the same fixed-amplitude reading is that the stiff component be at most comparable to the radiation density at big-bang nucleosynthesis, $T_{\mathrm{BBN}} \simeq 1\ \mathrm{MeV}$. An extra relativistic component of order the standard radiation density is the loosest requirement compatible with the light-element abundances [13]; the actual N_{eff} limits are tighter and only strengthen what follows. With the effective relativistic and entropy degrees of freedom made explicit, $g_*(T_{\mathrm{BBN}}) = g_{*s}(T_{\mathrm{BBN}}) = 10.75$ (photons, $e^\pm$, three neutrino species) and $g_{*s,0} = 3.91$, entropy conservation gives

$$\begin{aligned} a_{\mathrm{BBN}} &= \frac{T_0}{T_{\mathrm{BBN}}} \left(\frac{g_{*s,0}}{g_{*s}(T_{\mathrm{BBN}})} \right)^{1/3} \simeq 1.68 \times 10^{-10}, \\ \rho_r(T_{\mathrm{BBN}}) &= \frac{\pi^2}{30} g_* \frac{(k_B T_{\mathrm{BBN}})^4}{(\hbar c)^3} \simeq 7.4 \times 10^{25}\ \mathrm{J \cdot m^{-3}}, \end{aligned} \tag{47}$$

with $T_0 = 2.7255\ \mathrm{K}$ [12]. (The simple temperature-ratio estimate $a_{\mathrm{BBN}} \simeq T_0 / T_{\mathrm{BBN}} = 2.35 \times 10^{-10}$ differs by the order-unity $e^\pm$ entropy-transfer factor $\left(g_{*s,0}/g_{*s}\right)^{1/3} = 0.71$ and changes the final bound by a factor of about 1.5.) Requiring $K_\theta(a_{\mathrm{BBN}}) = K_\theta^{(0)} a_{\mathrm{BBN}}^{-6} \le f \rho_r(T_{\mathrm{BBN}})$ with $f \le 1$ gives

$$K_\theta^{(0)} \le f \rho_r(T_{\mathrm{BBN}}) a_{\mathrm{BBN}}^6 \simeq 1.6 \times 10^{-33} f\ \mathrm{J \cdot m^{-3}}, \tag{48}$$

which is $3 \times 10^{-24} f$ of the present dark-energy density, and hence, through Equation (50),

$$\sqrt{\zeta\kappa}\,\Omega_0 \le \Omega_{\mathrm{BBN}} \equiv \Omega_\Lambda \sqrt{\frac{f\rho_r\left(T_{\mathrm{BBN}}\right)a_{\mathrm{BBN}}^6}{\rho_\Lambda}} = 7.8\times10^{-30}\sqrt{f}\ \mathrm{s}^{-1}, \tag{49}$$

a factor $1.8\times10^{-12}\sqrt{f}$ below the present-background gate. At the stiff-PPN floor $\zeta = 1.7\times10^5$ this is $\sqrt{\kappa}\Omega_0 \lesssim 1.9\times10^{-32}\ \mathrm{s}^{-1}$; a present rotation rate of order H_0 would then require $\kappa \lesssim 8\times10^{-29}$, and the locked critical curvature would satisfy $m_c \lesssim 4\times10^{-40}\ \mathrm{m}^{-1}$. These are order-of-magnitude benchmarks: the choice $f = 1$, the neglect of the neutrino-decoupling details, and the use of a single temperature T_{BBN} each introduce order-unity uncertainties, none of which affects the twelve-order-of-magnitude gap between Equation (49) and the present-day gate.

Consequences for the gate. Within the minimal complex Pathway-B completion and with cosmologically constant $\hat{t}_\infty$ and κ, the rotating solution is *not* compatible with the cosmological evolution of its conserved charge unless the present rate satisfies the far stronger Equation (49); the numbers quoted in Eqs. (52)-(54) and in Corollary 6.1 should be read as present-day necessary conditions only. The loopholes are precisely the open items already listed in Section 10: a) a cosmological evolution of the amplitude $\hat{t}_\infty(a)$ or of $\kappa(a)$, which the series does not specify and which would alter Equation (46); b) late generation of the phase charge, so that $a^3 n$ is not conserved back to nucleosynthesis; or c) a stress-cancellation sector. We note in passing that a present-day coincidence $\Omega_0 \sim H_0$ (Section 5) cannot be a fixed relation, because $\Omega \propto a^{-3}$ while $H \propto a^{-3/2}$ during matter domination. None of these observations affects the strong-field results of Section 9, which use only the present-day stress: a tighter cosmological bound moves the locked $m_c r_s$ values of Section 9 further below unity and therefore reinforces the regime separation of Theorem 9.1.

Using Paper 7's ζ parameter gives

$$K_\theta = \frac{\zeta\kappa c^2\Omega^2}{16\pi G}. \tag{50}$$

Assumption 3.3 therefore requires

$$\sqrt{\zeta\kappa}\,\Omega \le \Omega_\Lambda \equiv \sqrt{\frac{16\pi G\rho_\Lambda}{c^2}} = 4.44790\times10^{-18}\ \mathrm{s}^{-1}. \tag{51}$$

At the unscreened stiff-PPN floor $\zeta = 1.7\times10^5$ of Paper 7,

$$\sqrt{\kappa}\,\Omega \le 1.0788\times10^{-20}\ \mathrm{s}^{-1}. \tag{52}$$

Thus $\Omega \sim H_0$ requires $\kappa \lesssim 2.44\times10^{-5}$ at that floor (**Figure 2**). This is mathematically allowed because the regular-vacuum normalisation of κ is not fixed by the series, but it is a new hierarchy requiring microscopic explanation.

If the Lock is imposed, Equation (51) becomes

$$m_c \le \frac{2\pi\Omega_\Lambda}{c\sqrt{\zeta}}. \tag{53}$$

At $\zeta = 1.7\times10^5$,

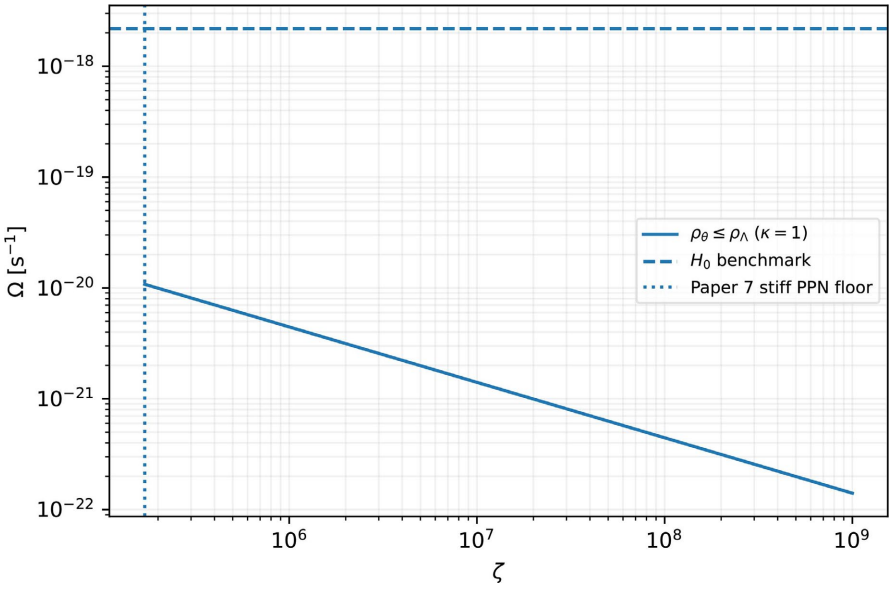


Figure 2. No-cancellation energy ceiling for $\kappa = 1$. The allowed region lies below the curve. The vertical line is the approximate Pathway-B stiff-PPN floor.

$$m_c \le 2.261\times10^{-28}\ \mathrm{m}^{-1},\quad m_c^{-1} \ge 4.42\times10^{27}\ \mathrm{m}. \tag{54}$$

Generic Yukawa screening is consequently unavailable unless the double-well shape is tuned extremely close to the lower edge where $\xi_\infty \to 0$.

A microscopic Compton-rate vacuum is much more problematic. For the electron, $\Omega_e = m_e c^2/\hbar = 7.7634\times10^{20}\ \mathrm{s}^{-1}$, and Equation (50) at $\zeta = \kappa = 1$ exceeds ρ_Λ by 3.05×10^{76}. A constant negative offset cannot cancel the full stress: setting $V_0 \simeq -K_\theta$ makes $\varepsilon_{\mathrm{vac}}$ small but leaves $p_{\mathrm{vac}} \simeq 2K_\theta$. A microscopic rotating vacuum therefore needs a dynamical stress-cancellation mechanism or a modified gravitational coupling; it is not repaired by the usual cosmological-constant subtraction alone.

6.2. Frequency-Dependent Phase-Amplitude Mixing

At asymptotic vacuum define $\chi = \sqrt{\kappa}\,\hat{t}_\infty \delta\theta$. The Paper-8 linear system can be written

$$\begin{pmatrix} D - M^2 & -iq \\ iq & D \end{pmatrix}\begin{pmatrix} \delta\hat{t} \\ \chi \end{pmatrix} = \begin{pmatrix} J \\ 0 \end{pmatrix},\quad q = \frac{2\sqrt{\kappa}\,\Omega\omega}{c^2}. \tag{55}$$

The amplitude spectral weight of the phase-like branch is

$$W_-^{(\hat{t})} = \frac{1}{2}\left(1 - \frac{M^2}{\sqrt{M^4 + 4q^2}}\right). \tag{56}$$

It scales quadratically for $q \ll M^2$ but tends to 1/2 for $q \gg M^2$. Thus Paper 8's $O\left(\omega/\omega_{\mathrm{gap}}\right)$ statement is a low-frequency expansion and does not imply a divergent coupling when the gap is cosmological. The source strength is redistributed among two mixed modes. Existing scalar-tensor binary bounds therefore do

not automatically remove the stiff-coupling branch, although compact-object sensitivities and the full complex-background PPN problem remain open [14].

Corollary 6.1 (Gravitational viability gate, present background). Without an additional stress-cancellation sector, a charged Pathway-B vacuum that uses the unscreened stiff route must satisfy approximately

$$\zeta \gtrsim 1.7\times 10^{5},\ \sqrt{\zeta\kappa}\,\Omega_0 \lesssim 4.4479\times 10^{-18}\ \mathrm{s}^{-1}\ \left(\text{present epoch, necessary}\right). \tag{57}$$

If Equation (2) is also imposed, its critical curvature is cosmological, Equation (53). If in addition the asymptotic amplitude and κ are cosmologically constant, so that the conserved charge redshifts as in Equation (46), the gate is superseded by the nucleosynthesis condition (49), $\sqrt{\zeta\kappa}\,\Omega_0 \lesssim 7.8\times 10^{-30}\ \mathrm{s}^{-1}$.

7. Four-Channel Matching at the Timeon Horizon

Paper 8 derived the local system

$$\left(D-M^2\right)\delta\hat{t} - 2i\kappa\hat{t}_0 a\Omega\omega\delta\theta = 0, \tag{58}$$

$$\hat{t}_0 D\delta\theta + 2ia\Omega\omega\delta\hat{t} = 0, \tag{59}$$

with $D = a\omega^2 - bk^2$, $a = \left(N^2c^2\right)^{-1}$, $b = N^2$, and

$$M^2 = \frac{V''\left(\hat{t}_0\right)}{Z_t} - \kappa a\Omega^2. \tag{60}$$

Define $q_\theta = \sqrt{\kappa}\hat{t}_0\delta\theta$ and $\Psi = \left(\delta\hat{t}, q_\theta\right)^{\mathrm{T}}$. Under Assumption 3.4, the radial problem is

$$\Psi'' + \boldsymbol{K}\left(r\right)\Psi = 0, \tag{61}$$

where

$$b\boldsymbol{K} = \begin{pmatrix} a\omega^2 - M^2 & -i\gamma \\ i\gamma & a\omega^2 \end{pmatrix},\quad \gamma = 2\sqrt{\kappa}\,a\Omega\omega. \tag{62}$$

The matrix is Hermitian, so

$$J = \mathrm{Im}\left(\Psi^{\dagger}\Psi'\right) \tag{63}$$

is conserved. The outer open channel is phase dominated and the outer amplitude partner is evanescent for the frequencies considered; inside, the D_- branch is amplitude dominated and propagating while the phase-dominated D_+ partner is evanescent. The matching therefore contains incident and reflected outer waves, a transmitted inner wave, and partner solutions on both sides whose termination must be specified.

7.1. Locked Background and Local Quantities

For the actual locked double well the background is constructed as follows (script paper9_model.py). In units of $\hat{t}_\infty$ the potential is $V = Z_t\hat{t}_\infty^2\mu^2 f\left(x\right)$ with

$f(x)=\left(x^2-u^2\right)^2\left(x^2-w^2\right)^2$, $u=v_{\mathrm{vac}}/\hat{t}_\infty$, $w=v_{\mathrm{atom}}/\hat{t}_\infty=\rho u$, and $\rho\equiv v_{\mathrm{atom}}/v_{\mathrm{vac}}$ the shape parameter. The homogeneous amplitude equation, Equation (24) with $(\nabla\theta)^2=-\Omega^2/c^2$, fixes $\mu^2 f'(1)=\kappa\Omega^2/c^2$, and the Lock fixes $\mu^2 f''(2\pi)=m_c^2=4\pi^2\kappa\Omega^2/c^2$; their ratio, $f''(2\pi)/f'(1)=4\pi^2$, determines u for given ρ (the root continuously connected to $u\to 1$). This reproduces every anchor quoted earlier: $\rho=12.58613$ gives $w=12.25502$ and $\xi_\infty=1.0000$; locked solutions exist exactly for $12.09319<w<15.84781$; and at the large-ρ asymptote $c_s^\infty=0.57502c$ and $r_{\mathrm{crit}}^{\mathrm{fr}}=1.5061r_s$. On the tracking profile $\hat{t}_0=\hat{t}_\infty/N$ the local mass is

$$M^2(r)=\mu^2 f''\left(1/N(r)\right)-\frac{\kappa\Omega^2}{N(r)^2c^2}, \tag{64}$$

which vanishes at $N_c=1/(2\pi)$, *i.e.* $r_c=1.0259886r_s$ for every shape, and equals $-C$ (with $C=\kappa a\Omega^2$) at the inflection radius r_{inf} where $V''=0$; r_c-r_{inf} is $1.2\times10^{-3}r_s$ for $\rho=13$ and $1.1\times10^{-2}r_s$ for $\rho=400$. Below r_{inf} the tracking amplitude passes through the atomic minimum and M^2 becomes positive again near $r\simeq1.006r_s$; the reduced model is not used there.

7.2. Numerical Methods for the Interface and Spinodal Calculations

Two length scales. The conversion layer, where $|M^2|\lesssim S=4\sqrt{\kappa}a\Omega\omega$ and the channels mix, has $u\equiv-M^2/C\lesssim S/C=8\pi(\omega r_s/c)/(m_c r_s)$, *i.e.* a width of order $10^{-3}(r_c-r_{\mathrm{inf}})/(m_c r_s/10^4)$. Outside it the amplitude-dominated channel has wavenumber or decay rate of order $\sqrt{|M^2|}/N\sim m_c$, but the phase-dominated channel does not: its outer wavenumber is $k_+\simeq(\omega/N^2c)\sqrt{1+4/m}$ with $m=M^2/C$, and its inner decay rate is $q_p\simeq(\omega/N^2c)\sqrt{4/u-1}$, both of order $10^2/r_s$ in the layer region. Consequently the phase-dominated channel is *not* adiabatic within a distance $\sim r_s$ of the horizon on either side: $q_p(r_c-r_{\mathrm{inf}})\simeq0.1$ for $\rho=13$, so the phase partner does not decay across the entire spinodal layer. Two consequences follow. First, an outer boundary condition cannot be imposed by projecting on local eigenvectors near the layer; the open channel must be carried out to an adiabatic radius. Second, a "decaying partner" condition imposed anywhere inside the spinodal layer is a modelling choice, not an asymptotic condition, and its influence must be quantified.

Outer zone and hand-off. For $r\geq r_1$ the evanescent amplitude channel is eliminated adiabatically and the open channel obeys the scalar equation $\phi''+\lambda_+(r)\phi=0$ with λ_+ the larger eigenvalue of $\boldsymbol{K}(r)$; the neglected eigenvector-rotation terms are of relative size $|\mathrm{d}\hat{v}_+/\mathrm{d}r|/q_-\leq1.5\times10^{-4}$ at r_1 for all runs. Incident and reflected solutions are started at $R_{\mathrm{far}}=100r_s$ with first-order WKB data $\phi=k^{-1/2}\mathrm{e}^{\mp\mathrm{i}\int k\mathrm{d}r}$, $k=\sqrt{\lambda_+}$, and integrated inward to r_1. The hand-off

radius r_1 is placed where the evanescent amplitude channel has $q_-(r_1 - r_c) = 20$ e-folds to the horizon ($r_1 - r_c$ between $5.1\times10^{-4} r_s$ at $m_c r_s = 10^4$ and $2.3\times10^{-5} r_s$ at 10^6).

Near zone and inner termination. On $[r_{\text{in}}, r_1]$ the full coupled system (61) is integrated as a four-dimensional complex first-order system with no local diagonalisation, so that mode conversion is computed rather than approximated. From r_1 the incident and reflected solutions (local eigenvector $\hat{v}_+(r_1)$ times the scalar data) and the outward-decaying evanescent solution ($\hat{v}_-$, $\Psi' = -q_-\Psi$) are integrated inward to r_c; from r_{in} the two inner-admissible solutions are integrated outward to r_c. Each direction integrates the physically growing member of every evanescent pair, so the integration is stable and the matching matrix is column-scaled. The inner amplitude-dominated channel is always an inward WKB wave (nothing returns from the interior). For the phase-dominated partner three terminations are used: (E) the decaying local eigen-solution at r_{in}, $\Psi' = +q_p\Psi$, which is the condition used in an earlier draft of this analysis; (Q) the dense-stratum phase quench of Papers 4-6, $\delta\theta(r_{\text{in}}) = 0$, with the admissible pair constructed exactly from the local channel vectors so that $\Psi_2(r_{\text{in}}) = 0$; and (N) the Neumann condition $\delta\theta'(r_{\text{in}}) = 0$. The termination radius is parametrised by $u_{\text{w}} = u(r_{\text{in}})$; $u_{\text{w}} = 0.95$ is essentially the inflection radius and $u_{\text{w}} = 12S/C$ places the termination at the inner edge of the conversion layer, a distance $\propto (m_c r_s)^{-1}$ inside the horizon that shrinks with the layer; we call this the *layer-tracking quench*. It is not the limit $u_{\text{w}} \to 0$, which would put the condition inside the mode-conversion zone itself; it is the closest termination to the horizon that still lies outside that zone, and the two differ only by a fixed multiple of the layer thickness.

Matching, fluxes, and integrator. The 4×4 complex system $c_t Y_t + c_p Y_p = Y_{\text{inc}} + R\,Y_{\text{ref}} + B\,Y_{\text{ev}}$ is solved at r_c. The transmitted flux is read from the full matched solution at r_{in}, $T = |J(r_{\text{in}})| / |J_{\text{inc}}|$, which includes the cross-flux of the partner pair under conditions (Q) and (N); $|R|^2$ is read from the reflected amplitude, and $T + |R|^2 - 1$ is the flux residual. The integrator is scipy.integrate.solve_ivp with DOP853 at relative tolerance 10^{-10} and absolute tolerance 10^{-13}.

Convergence. For each of the five terminations of Table 5 and for $m_c r_s = 10^4$ and 10^6, T changes by at most 7.7×10^{-4} (relative) when the hand-off is moved from 20 to 10 or 30 e-folds, by at most 1.2×10^{-4} when R_{far} is moved from $100 r_s$ to $50 r_s$ (and by 1.9×10^{-5} to $200 r_s$), by at most 1.1×10^{-6} when the tolerances are tightened by 10^2, and by at most 2.8×10^{-7} when DOP853 is replaced by RK45 (70 runs, file paper9_four_channel_convergence.csv). Flux residuals are $\le 7\times10^{-8}$ for every entry of Table 5, Table 6; within the convergence scan they rise to 1.7×10^{-5} only for the Neumann termination at the 30-e-fold hand-off, where the evanescent column has grown by e^{30}. The exponent statements below are finite-difference slopes of $\ln T$ against $\ln(m_c r_s)$.

Spinodal proxy. The attenuation proxy (68) is a one-dimensional quadrature

over $[r_{\mathrm{inf}}, r_c]$ (script paper9_spinodal_window_scan.py). Both end points are located by Brent's method to $10^{-15} r_s$: r_c as the root of M^2 (and checked against the analytic $1.0259886 r_s$) and r_{inf} as the first root of $V''(\hat{t}_0(r))$ below r_c. The integrand uses the analytic $\Gamma_{\max}$ of Equation (67) and the group velocity of the propagating inner branch, $y_-(z) = z + u/2 + \sqrt{u^2 + 16z}/2$ with $z = a\omega^2/C$, obtained by implicit differentiation of the secular equation: $v_g = N^2\sqrt{y/z}\,(\mathrm{d}z/\mathrm{d}y)c$. The integrand has an integrable $u^{-1/2}$ singularity at r_c (where $v_g \to \infty$ as $u \to 0$); it is removed by the substitution $r = r_c - t^2$ and the result integrated with adaptive Gauss-Kronrod (scipy.integrate.quad, relative tolerance 10^{-10}, error estimates $\le 10^{-11}$). An independent composite Simpson rule on 4001 points agrees to all five printed figures, halving the tolerance changes nothing at 10^{-13}, and because $z = 4\pi^2(\omega r_s/c)^2/(m_c r_s)^2 \ll 1$ the values are insensitive to $m_c r_s$ (they change by 4% between $m_c r_s = 10^6$ and 10^4). No evanescent channel enters this quadrature.

7.3. Results

Table 5. Four-channel transmitted flux for $v_{\mathrm{atom}}/v_{\mathrm{vac}} = 13$ and $\omega r_s/c = 1$ under the inner terminations of Section 7.2: (N) Neumann partner at r_{inf}; (E) decaying partner seeded at $u_{\mathrm{w}} = 0.03$; (Q) dense-stratum phase quench at r_{inf}, at $u_{\mathrm{w}} = 0.03$, and layer-tracking ($u_{\mathrm{w}} = 12S/C$, inner edge of the conversion layer). ϵ_{red} is the layer validity parameter of Equation (19). Flux residuals $\left|T + |R|^2 - 1\right| \le 7\times10^{-8}$ throughout.

$m_c r_s$	$\epsilon_{\mathrm{red}}^{\mathrm{layer}}$	T (N, r_{inf})	T (E, 0.03)	T (Q, r_{inf})	T (Q, 0.03)	T (Q, layer-tracking)
10^4	6.3×10^{-3}	0.7446	0.03307	6.427×10^{-3}	2.07×10^{-5}	2.07×10^{-5}
3×10^4	3.6×10^{-3}	0.7330	0.01992	6.405×10^{-3}	6.40×10^{-6}	4.86×10^{-6}
10^5	2.0×10^{-3}	0.7166	0.03037	6.398×10^{-3}	6.06×10^{-6}	1.06×10^{-6}
3×10^5	1.1×10^{-3}	0.7193	0.02833	6.399×10^{-3}	5.91×10^{-6}	2.73×10^{-7}
10^6	6.3×10^{-4}	0.7212	0.02915	6.400×10^{-3}	6.06×10^{-6}	6.36×10^{-8}
slope $10^5 \to 10^6$		+0.003	−0.017	+0.0002	+0.0002	−1.22

Three features of Table 5 and Figure 3 are robust. 1) For every termination imposed at a fixed physical radius, T is independent of $m_c r_s$: the fitted slopes between 10^5 and 10^6 are below 0.02 in magnitude, and the residual variation at 10^4–3×10^4 is of the size expected from ϵ_{red}. 2) The value of T is set almost entirely by the termination: it ranges from 0.72 (Neumann) through 0.03 (decaying seed) and 6.4×10^{-3} (quench at the inflection radius) to 6×10^{-6} (quench at $u_{\mathrm{w}} = 0.03$). For the quench the dependence on the termination radius is a clean power law, $T \simeq 7\times10^{-3} u_{\mathrm{w}}^2$ for u_{w} outside the conversion layer (file paper9_four_channel_wallscan.csv). 3) Only for the layer-tracking quench, whose termination moves inward with the layer as m_c grows, does T decrease with curvature, with local slopes −1.32, −1.27, −1.23, −1.21 across the table.

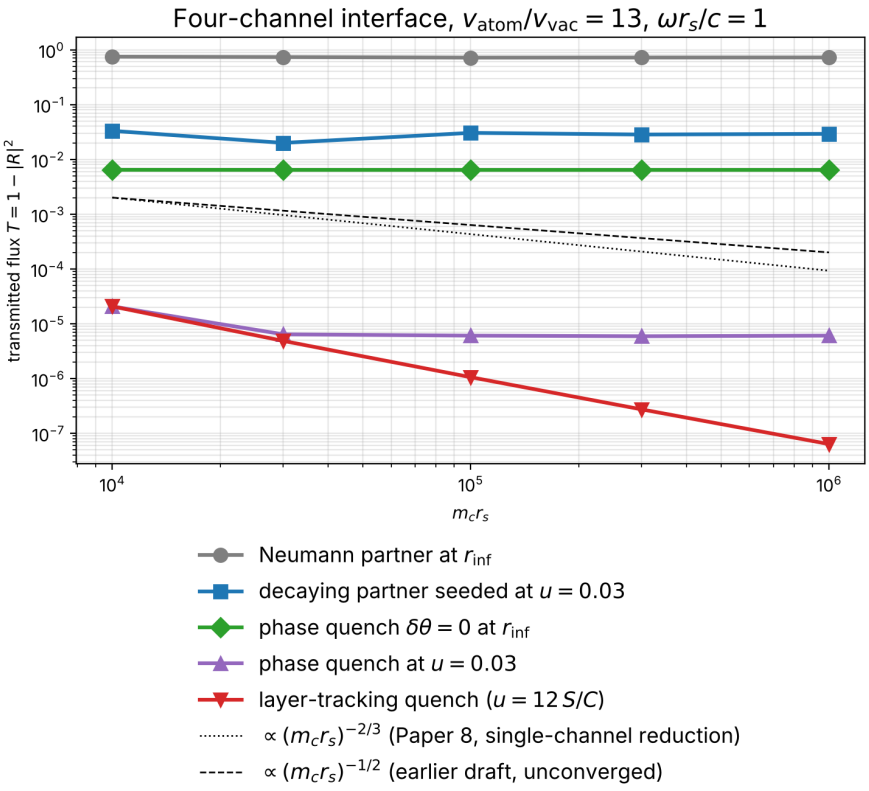


Figure 3. Four-channel transmitted flux for the locked $v_{atom}/v_{vac} = 13$ double well at $\omega r_s/c = 1$ under the five inner terminations of Table 5. For any termination at a fixed physical radius the flux is independent of $m_c r_s$; only the layer-tracking quench, whose position moves inward with the conversion layer, produces a curvature-dependent, and much steeper, suppression. The dotted and dashed lines show the −2/3 law of Paper 8's single-channel reduction and the −1/2 law of an earlier draft's unconverged partner treatment for comparison; neither is realised.

Table 6. Transmitted flux with the layer-tracking dense-stratum quench ($u_w = 12S/C$, inner edge of the conversion layer) across the locked double-well family and two frequencies.

v_{atom}/v_{vac}	$\omega r_s/c$	$T(m_c r_s = 10^4)$	$T(10^5)$	$T(10^6)$
13	1	2.1×10^{-5}	1.1×10^{-6}	6.4×10^{-8}
13	3	2.3×10^{-3}	4.9×10^{-5}	2.2×10^{-6}
20	1	3.4×10^{-3}	6.2×10^{-5}	2.6×10^{-6}
20	3	0.91	3.4×10^{-2}	2.9×10^{-4}
30	1	2.4×10^{-2}	2.3×10^{-4}	8.1×10^{-6}
30	3	0.99	0.20	1.4×10^{-3}
100	1	0.10	7.0×10^{-4}	1.9×10^{-5}
100	3	1.00	0.54	5.1×10^{-3}

Table 6 shows that even the layer-tracking quench is not a universal mirror over the scanned range: at $m_c r_s = 10^4$ and $\omega r_s/c = 3$ the broader shapes trans-

mit almost completely, because the layer between the horizon and the quench surface acts as a thin, partly transparent barrier for the phase channel, and the suppression only becomes strong ($T \lesssim 10^{-2}$ for every shape) at $m_c r_s \gtrsim 10^6$. The local exponents in this table range from −0.3 (where T is still near unity) to −2.2 and have not settled to a single value by $m_c r_s = 10^6$.

Theorem 7.1 (Four-channel interface transmission). Within the reduced radial approximation of Assumption 3.4, in the parameter region $(m_c r_s)(\omega r_s/c) \gtrsim 4\times 10^3$ where $\epsilon_{\mathrm{red}}^{\mathrm{layer}} \le 10^{-2}$: a) the transmitted flux through the timeon horizon is not fixed by the conversion layer; it is fixed by the termination of the phase-dominated partner channel inside the horizon, and for any termination at a fixed physical radius it is independent of $m_c r_s$, $\left|\mathrm{d}\ln T/\mathrm{d}\ln(m_c r_s)\right| < 0.02$ for $10^5 \le m_c r_s \le 10^6$; b) neither the $(m_c r_s)^{-2/3}$ law of Paper 8, which arose from the single-channel reduction, nor the $(m_c r_s)^{-1/2}$ law of an earlier draft of this analysis, which arose from an unconverged "decaying partner" treatment of a channel whose decay length exceeds the layer thickness, is realised by any termination; c) near-total reflection follows only from the dense-stratum phase quench $\delta\theta = 0$ of Papers 4-6, with $T \simeq 7\times 10^{-3} u_w^2$ for a quench at fixed u_w and $T \le 6\times 10^{-8}$ - 5×10^{-3} at $m_c r_s = 10^6$ across the locked family for the layer-tracking quench.

The physical reading is that the timeon horizon of the reduced model is a mode-conversion surface, not a mirror. The amplitude-dominated channel always transmits into the spinodal region, and the phase-dominated channel tunnels through the thin spinodal layer unless the dense stratum quenches it. The Chrono-Quantum Mirror of Paper 2 is therefore identified, within this model, with the phase quench of the dense stratum rather than with the thin-interface mode matching of Paper 8, and its reflectivity depends on how sharply that quench sets in at $\hat{t} = \hat{t}_{\mathrm{crit}}$. This strengthens the link to Papers 4-6 but weakens the claim that reflection is a consequence of curvature alone. A fully covariant spherical perturbation equation, and a model of the interior that fixes the phase impedance, remain future calculations.

8. Where the Absorption Is

Inside the timeon horizon write

$$M^2 = -uC,\ C \equiv \kappa a \Omega^2,\ 0 < u \le 1. \tag{65}$$

Let $x = a\omega^2$, $y = bk^2/C$, and $z = x/C$. The Paper-8 secular equation becomes

$$(z-y)^2 + u(z-y) - 4z = 0. \tag{66}$$

For the unstable root, direct optimisation with respect to y gives

$$y_* = \frac{u}{2} - \frac{u^2}{16},\quad \boxed{\Gamma_{\max} = \sqrt{-\omega_-^2} = \frac{\sqrt{\kappa}\Omega}{4}u = \frac{\left|M^2\right|}{4\sqrt{\kappa}a\Omega}.} \tag{67}$$

Under Assumption 3.5, the optimistic optical-depth proxy is

$$\alpha_{\mathrm{sp}}(\omega)=\int_{r_{\mathrm{inf}}}^{r_c}\frac{\Gamma_{\max}(r)}{\left|v_g^{(-)}(r,\omega)\right|}\mathrm{d}r. \tag{68}$$

The calculation uses the actual locked double-well $M^2(r)$ and the exact finite-frequency group velocity; the results are given in Table 7; the quadrature, end-point treatment, and convergence tests are described in Section 7.2.

The calculation in this section is deliberately a test of the same locked high-curvature tracking branch used by the interface calculation. It is not a calculation of the low-curvature uncancelled branch identified in Section 9, for which the thin transition-layer approximation is unavailable. The result below is therefore a branch-specific negative result: even the branch most favourable to a narrow mirror does not obtain the required attenuation from the linear layer alone.

Paper 2 requires

$$G=\sqrt{R_{\mathrm{bar}}R_{\mathrm{bnd}}}\,\mathrm{e}^{-\alpha}<10^{-3}. \tag{69}$$

With $R_{\mathrm{bnd}}\simeq 1$, this is $\mathrm{e}^{-2\alpha}R_{\mathrm{bar}}<10^{-6}$. For $R_{\mathrm{bar}}=1$ the requirement is $\alpha>\ln 1000=6.90776$, while the largest executed value is 3.65465 (Figure 4).

Table 7. Optimistic spinodal optical depth at $m_c r_s=10^6$.

$v_{\mathrm{atom}}/v_{\mathrm{vac}}$	$\alpha_{\mathrm{sp}}(\omega r_s/c=1)$	$\alpha_{\mathrm{sp}}(\omega r_s/c=3)$
13	0.1032	0.3087
20	0.5962	1.7827
30	0.8923	2.6679
100	1.1892	3.5550
400	1.2225	3.6547

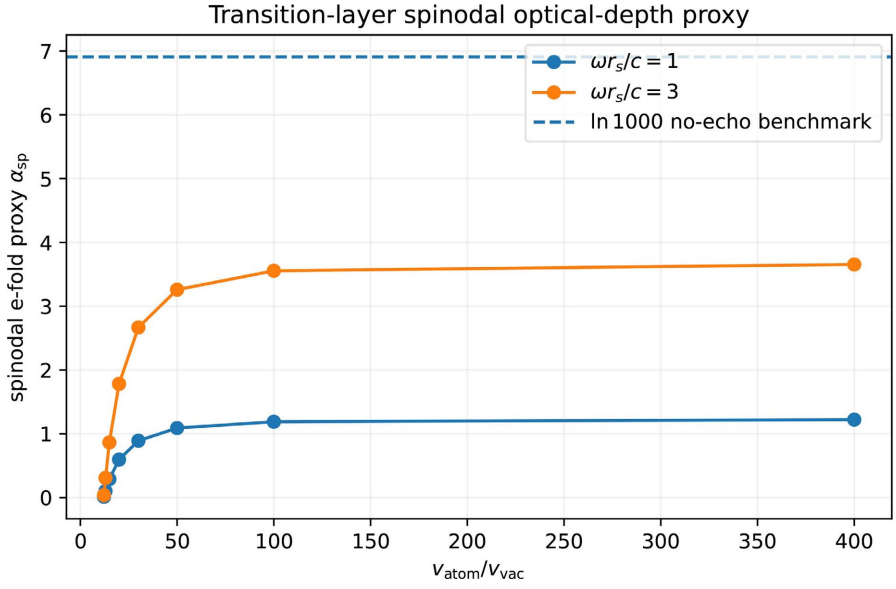


Figure 4. Optimistic spinodal optical-depth proxy across the locked double-well family at $m_c r_s=10^6$. The conservative no-echo benchmark $\ln 1000$ is not reached.

Theorem 8.1 (The linear transition layer is insufficient). Even when every fastest-growing spinodal e-fold is counted as irreversible attenuation, the horizon-to-inflection layer does not satisfy Paper 2's conservative no-echo inequality for order-unity barrier reflectivity over the executed locked-window scan with $\omega r_s/c \le 3$. The dense-time interior, nonlinear phase conversion, or another dissipative sector must supply the remaining attenuation.

This is a one-sided result: linear spinodal growth is not itself absorption. Treating it as attenuation is intentionally generous, so the shortfall cannot be repaired merely by reinterpreting the same conservative instability rate as dissipation.

9. Strong-Field Pathway-B Exterior and Branch Separation

Paper 7 obtains exact Schwarzschild in Pathway B when $\hat{t}$ is constant at a real vacuum with zero vacuum energy. Under Assumption 3.2, however, $\theta = \Omega t$ contributes nonzero stress, so Birkhoff's vacuum theorem no longer proves exact Schwarzschild. The stress bound nevertheless makes the metric correction minute on black-hole scales.

Combining Equation (53) with $r_s = 2GM/c^2$ gives the maximum locked $m_c r_s$ in the no-cancellation branch (Table 8). By contrast, Paper 8's sudden-interface calculation requires $m_c r_s \gg 10^3$.

Table 8. Maximum $m_c r_s$ allowed by the no-cancellation phase-stress bound if the Lock is imposed.

$M/M_\odot$	$m_c r_s$ max ($\zeta = 1$)	$m_c r_s$ max ($\zeta = 1.7\times10^5$)
30	8.26×10^{-21}	2.00×10^{-23}
10^6	2.75×10^{-16}	6.68×10^{-19}
10^{10}	2.75×10^{-12}	6.68×10^{-15}

Theorem 9.1 (Mirror/gravity regime separation). If the no-cancellation phase-stress bound and the Spectral Lock are both imposed, no astrophysical black hole lies in the high-$m_c r_s$ thin-interface regime used by the Paper-8 mirror calculation. The microscopic-curvature mirror branch therefore requires either stress cancellation, modified phase gravitation, or abandonment of the no-cancellation benchmark; it is not the same branch as the uncancelled gravitationally viable Lock.

The metric itself remains almost Schwarzschild in the viable branch: even for $10^{10} M_\odot$, the phase-stress correction on the scale r_s, $8\pi G\rho_\Lambda r_s^2/c^4$, is bounded at roughly 10^{-25}. What remains nontrivial is the scalar amplitude profile. Pathway B treats $g_{\mu\nu}$ and $\hat{t}$ as independent fields, and Equation (24) does not imply the Paper-8 tracking law $\hat{t} = \hat{t}_\infty/N$.

Two controlled limiting diagnostics illustrate the ambiguity. In the adiabatic-tracking limit, the Lock gives $N = 1/(2\pi)$ and hence

$$\frac{r_{\mathrm{crit}}^{\mathrm{track}}}{r_s}=\frac{1}{1-(2\pi)^{-2}}=1.0259886. \tag{70}$$

In a locally frozen-amplitude limit the bare curvature remains approximately $m_{s,\mathrm{bare}}^2$, so

$$N_{\mathrm{fr}}=N_c\sqrt{\xi_\infty},\quad \frac{r_{\mathrm{crit}}^{\mathrm{fr}}}{r_s}=\frac{1}{1-N_{\mathrm{fr}}^2}. \tag{71}$$

Across the locked double-well family this diagnostic ranges from $1.001r_s$ near the lower edge ($v_{\mathrm{atom}}/\hat{t}_\infty=12.10$) to $1.506r_s$ at the large-v_{atom} asymptote (Figure 5).

Theorem 9.2 (Strong-field Pathway-B gate). The existing series does not uniquely determine the Pathway-B timeon-horizon radius once the rotating phase is included. In the no-cancellation branch the phase stress is too small to move the Schwarzschild metric appreciably, but the amplitude equation remains an independent global boundary-value problem. Therefore $r_{\mathrm{crit}}=1.02599r_s$ is an adiabatic-tracking limit, not a derived Pathway-B strong-field prediction.

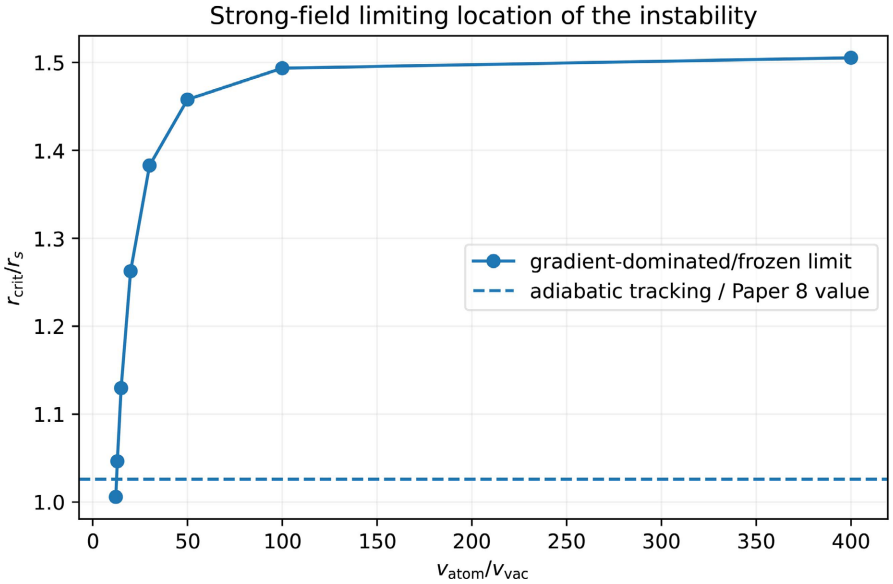


Figure 5. Two controlled diagnostics for the instability radius on an effectively Schwarzschild metric. The horizontal line is the Paper-8 adiabatic-tracking value. The curve is the locally frozen-amplitude diagnostic. They are not asserted to form a rigorous bracket for every global scalar boundary condition.

Equations (70) and (71) are diagnostic limits, not a proven bracket. A rigorous bracket would require monotonicity or maximum-principle control of the nonlinear scalar boundary-value problem, together with cosmological boundary data when the scalar curvature length is itself cosmological.

10. Discussion: What Paper 9 Establishes

The central result is not a preferred numerical factor but a consistency map. Four

quantities that were previously treated separately are linked:

$$\boxed{\text{lattice density} \leftrightarrow \Omega \leftrightarrow \text{vacuum stress} \leftrightarrow m_c \leftrightarrow \text{interface regime.}} \tag{72}$$

A microscopic theory cannot select one element of this chain independently of the rest.

First, the 2π value remains special but unexplained. The series gives an exact equivalence between the Lock and a primitive-cell density, Equation (35). That is progress: the missing physics has been localised. But the BPS does not provide it, dense-time saturation does not provide it, and a natural asymptotic-curvature cell law still leaves the potential shape free.

Second, the phase rotation is not gravitationally innocuous. In the minimal complex Pathway-B action it is a stiff positive-energy source. A Hubble-scale numerical coincidence can occur in a proton-sized excess-charge benchmark, but the phase component does not behave as dark energy. The unscreened stiff route further constrains the allowed rate. Moreover, the present-background gate is only a necessary condition: with cosmologically constant amplitude and stiffness, the conserved charge redshifts stiffly and the same vacuum would have dominated the matter and radiation eras unless its present rate is some twelve orders of magnitude below the gate (Section 6.1). Either the amplitude or the charge must have a cosmological history that the series has not yet specified, or a cancellation sector is required. Conversely, a microscopic Compton-rate vacuum demands a new stress-cancellation mechanism whose tensor structure is more specific than a vacuum-energy subtraction.

Third, the reflective interface is not a consequence of curvature. With all four channels retained and the open channel carried to an adiabatic boundary, the transmitted flux through the timeon horizon is independent of $m_c r_s$ and is fixed by how the phase-dominated partner is terminated inside the horizon; the −2/3 law of Paper 8's single-channel reduction and the −1/2 law of an earlier draft's unconverged partner treatment are both absent. Near-total reflection is obtained only from the dense-stratum phase quench of Papers 4-6, and its strength depends on how sharply that quench sets in at $\hat{t} = \hat{t}_{\text{crit}}$. The Chrono-Quantum Mirror is therefore a property of the dense stratum, not of the thin interface. Where reflection does occur it makes the no-echo problem harder rather than easier: the linear transition layer does not demonstrate enough irreversible loss.

Fourth, the strong-field problem splits into branches. A microscopic-curvature branch can support the sudden-interface approximation but requires additional gravitational physics for the rotating vacuum. The uncancelled branch permitted by the energy bound has cosmological curvature and cannot use the same interface asymptotics. In that branch the metric is essentially Schwarzschild but the scalar profile is not locally determined by the lapse.

10.1. Derived, Postulated, Numerical, and Open

Table 9 and Table 10 record the status of every principal statement of this paper

Table 9. Status of the principal Paper-9 statements: lattice, closure, and gravitational results (continued in **Table 10**).

Statement	Status
$n = Z_t \kappa \hat{t}_\infty^2 \Omega / \left(\hbar c^2\right)$	Derived from Noether charge of the compact $U(1)$ (Definition 4.1)
$\ell^3 = 8\pi c \ell_{\mathrm{P}}^2 / \left(\zeta \kappa \Omega\right)$ for one quantum/cell	Derived conditional on occupancy definition
Spectral Lock follows from Papers 1-8	**No**
Asymptotic Lattice-Density Postulate, Equation (40)	Candidate postulate; tested, not adopted
Charged phase gravitates in minimal complex Pathway B	Derived
No-cancellation energy ceiling Equation (51)	Derived from Assumption 3.3; present epoch, necessary only
Nucleosynthesis-era bound Equation (49)	Derived, conditional on constant $\hat{t}_\infty$, κ and conserved $a^3 n$
Rotating vacuum compatible with cosmological charge evolution at the present-gate rate	**No** under fixed amplitude; open otherwise
High-frequency mixing saturates rather than diverges	Derived from two-mode matrix

Table 10. Status of the principal Paper-9 statements, continued: interface, absorption, and strong-field results.

Statement	Status
Four-channel transmission is a power law in $m_c r_s$ (−2/3 or −1/2)	**No**; numerical, reduced radial model, valid for $\left(m_c r_s\right)\left(\omega r_s / c\right) \gtrsim 4 \times 10^3$
Transmission fixed by interior phase-channel termination; near-total reflection requires the dense-stratum quench	Numerically converged within the reduced radial model
$\Gamma_{\max} = \sqrt{\kappa}\,\Omega u / 4$	Derived analytically
Spinodal layer alone proves no echoes	**No**; numerical upper-envelope test
$1.02599 r_s$ is unique Pathway-B horizon radius	**No**; tracking limit
Exact global Pathway-B scalar profile	Open
Microscopic stress-cancellation mechanism	Open

10.2. The Minimum Additional Physics

A successful microscopic completion must supply at least two pieces of information that the present series leaves independent: a lattice-density law selecting n (hence Ω through Equation (31)) and a potential-shape selection or other dynamical relation fixing the ratio of critical to asymptotic curvature. It must then pass the gravitational-stress constraint. If it chooses microscopic Ω, it must also explain how the phase stress gravitates without overwhelming the observed background. If it chooses cosmological Ω, it must explain how a strong reflective boundary arises when $m_c r_s \ll 1$ or abandon the thin-interface mechanism. This is a substantially narrower target than the unconstrained Spectral Lock with which the paper began.

11. Conclusions

Paper 8 established that the CQM can be understood as a constitutive timeon horizon and isolated the Spectral Lock as the condition that recovers $\hat{t}_{\mathrm{crit}} = 2\pi/c$. Paper 9 has tested whether that condition follows from the rest of the series. It does not.

The exact charge-density relation converts the Lock into a microscopic lattice statement, but the primitive cell size is not fixed by Papers 1-8. The BPS does not quantise the vacuum frequency; dense-time saturation is not a number-density closure; no matter mass is selected as the vacuum clock; and a horizon-free Planck-plus-potential candidate still leaves the double-well shape free. The factor 2π is therefore a genuine selection datum, not an algebraic inevitability.

At the same time, the charged vacuum cannot be treated as a spectator. In the minimal complex Pathway-B completion it carries stiff positive stress, sharply constraining the allowed charge sector; and because that stress redshifts as a^{-6} under charge conservation, the present-day stress gate is a necessary condition whose cosmological extension is far more restrictive. The four-channel calculation shows that the interface transmission is set by the interior phase-channel termination rather than by curvature, so that the mirror is the dense-stratum phase quench and not the thin interface; the linear spinodal layer does not provide enough demonstrated absorption to satisfy the conservative no-echo bound, and the uncancelled locked vacuum lies far outside the high-curvature mirror regime for astrophysical black holes. The familiar $1.026 r_s$ radius survives as the adiabatic-tracking value, not as a unique Pathway-B solution.

The critical time density has therefore been reduced to a precise next problem. A microscopic theory of the timeon substrate must determine the primitive lattice density and potential shape, and it must do so in a charge sector whose gravitational stress, interface structure, interior dissipation, and global strong-field profile are mutually consistent. That is the remaining route by which $2\pi/c$ can become a prediction rather than a postulate.

Conflicts of Interest

The author declares no conflicts of interest regarding the publication of this paper.

References

[1] Davey, G. (2026) Universum Probabile Altera. *Journal of High Energy Physics, Gravitation and Cosmology*, **12**, 126-137. https://doi.org/10.4236/jhepgc.2026.121007

[2] Davey, G. (2026) Beyond the Causal Diamond: A Probabilistic Model of Cyclical Quantum Gravity. *Journal of High Energy Physics, Gravitation and Cosmology*, **12**, 839-856. https://doi.org/10.4236/jhepgc.2026.122045

[3] Davey, G. (2026) Quantum Mechanics of the Timeon Field: Algebraic and Symplectic Framework for Quantum Gravity. *Journal of Applied Mathematics and Physics*, **14**, 1535-1586. https://doi.org/10.4236/jamp.2026.144073

[4] Davey, G. (2026) Dense Time Quantum Mechanics: Physics of the Dense-Time Collective Partner State. *Journal of High Energy Physics, Gravitation and Cosmology*, **12**, 1612-1642. https://doi.org/10.4236/jhepgc.2026.123081

[5] Davey, G. (2026) Algebraic Chrono-Dynamics: Stratified Covariant Phase Space and Boundary Algebra. *Journal of Applied Mathematics and Physics*, **14**, 2201-2237. https://doi.org/10.4236/jamp.2026.146108

[6] Davey, G. (2026) Global Stratified Reduction and Boundary Cohomology for Phase-Suppressed Covariant Field Theory. *Journal of Applied Mathematics and Physics*, **14**, 2164-2191. https://doi.org/10.4236/jamp.2026.146106

[7] Davey, G. (2026) General Relativity as the Einstein Limit of Time-Density. Preprint. Zenodo. https://doi.org/10.5281/zenodo.20090061

[8] Davey, G. (2026) The Chrono-Quantum Mirror as a Timeon Horizon. Version 9.5. Preprint. https://doi.org/10.5281/zenodo.23073563

[9] Unruh, W.G. (1981) Experimental Black-Hole Evaporation? *Physical Review Letters*, **46**, 1351-1353. https://doi.org/10.1103/physrevlett.46.1351

[10] Barceló, C., Liberati, S. and Visser, M. (2011) Analogue Gravity. *Living Reviews in Relativity*, **14**, Article No. 3. https://doi.org/10.12942/lrr-2011-3

[11] Cardoso, V. and Pani, P. (2019) Testing the Nature of Dark Compact Objects: A Status Report. *Living Reviews in Relativity*, **22**, Article No. 4. https://doi.org/10.1007/s41114-019-0020-4

[12] Planck Collaboration, Aghanim, N., *et al.* (2020) Planck 2018 Results. VI. Cosmological Parameters. *Astronomy & Astrophysics*, **641**, A6. https://doi.org/10.1051/0004-6361/201833910

[13] Fields, B.D., Olive, K.A., Yeh, T. and Young, C. (2020) Big-Bang Nucleosynthesis after Planck. *Journal of Cosmology and Astroparticle Physics*, **2020**, Article No. 010. https://doi.org/10.1088/1475-7516/2020/03/010

[14] Freire, P.C.C., Wex, N., Esposito-Farèse, G., Verbiest, J.P.W., Bailes, M., Jacoby, B.A., *et al.* (2012) The Relativistic Pulsar-White Dwarf Binary PSR J1738+0333—II. The Most Stringent Test of Scalar-Tensor Gravity. *Monthly Notices of the Royal Astronomical Society*, **423**, 3328-3343. https://doi.org/10.1111/j.1365-2966.2012.21253.x

[15] Coleman, S. (1985) Q-Balls. *Nuclear Physics B*, **262**, 263-283. https://doi.org/10.1016/0550-3213(85)90286-x

Appendix A. BPS Charge Correction and the Paper-3 Thin-Wall Caveat

Paper 3 uses a static spherical ansatz $\Phi = \hat{t}(r)\mathrm{e}^{\mathrm{i}\theta(r)}$ and integrates the radial phase equation to

$$r^2\hat{t}^2\theta'(r) = Q. \tag{A1}$$

This constant is a radial phase-current flux, not the temporal Noether charge. The conserved $U(1)$ charge is proportional to

$$N = \int j^0 \mathrm{d}^3x \propto \int \hat{t}^2\partial_t\theta \mathrm{d}^3x, \tag{A2}$$

which vanishes for the static phase ansatz.

There is also a regularity obstruction. Near a finite atomic core amplitude, the phase-gradient energy contains

$$4\pi\int_\epsilon \mathrm{d}r\, r^2 \frac{Q^2}{r^4\hat{t}^2} \sim \frac{4\pi Q^2}{v_{\mathrm{atom}}^2\epsilon}, \tag{A3}$$

which diverges as $\epsilon \to 0$, while $\theta \sim -Q/\left(rv_{\mathrm{atom}}^2\right)$ is unbounded. Finite energy and regularity therefore require $Q = 0$. A phase depending only on r has no angular winding on a spherical shell, so single-valuedness does not quantise Equation (A1).

The finite charged stationary replacement is Q-ball-like [15],

$$\Phi = \hat{t}(r)\mathrm{e}^{\mathrm{i}\Omega t}, \tag{A4}$$

with the same global Ω as the surrounding stationary condensate. Its excess charge is Equation (38); the BPS size determines ΔN once the vacuum sector is chosen and therefore does not select Ω.

For a homogeneous condensate, eliminating Ω in favour of n gives

$$\varepsilon(n,\hat{t}) = \frac{\hbar^2c^2n^2}{2Z_t\kappa\hat{t}^2} + V(\hat{t}). \tag{A5}$$

Minimising at fixed n produces the Paper-8 background equation and, by the envelope theorem,

$$\boxed{\frac{\partial\varepsilon}{\partial n} = \hbar\Omega.} \tag{A6}$$

This is the condensate chemical-potential identity and holds for every n; it cannot serve as a unit-charge vacuum-selection principle.

A separate Paper-3 bookkeeping issue concerns its thin-wall estimate. The printed polynomial

$$V = \lambda\left(\hat{t}^2 - v_{\mathrm{vac}}^2\right)^2\left(\hat{t}^2 - v_{\mathrm{atom}}^2\right)^2 \tag{A7}$$

has degenerate minima $V(v_{\mathrm{vac}}) = V(v_{\mathrm{atom}}) = 0$. Any thin-wall formula using $\Delta V = V(v_{\mathrm{atom}}) - V(v_{\mathrm{vac}}) < 0$ therefore requires an additional tilt/nondegeneracy term not present in the written potential. Paper 9 does not use that thin-wall energy difference in any derivation.

Appendix B. Reproducibility

Every numerical result introduced or recalculated in this paper is generated, or independently re-verified, by the scripts listed here, which are delivered with the manuscript together with their outputs (Python 3.11, NumPy, SciPy); inherited calibrations and literature constants are listed in Table 2.

- paper9_model.py: the locked double-well background of Section 7.1 (shape root $u(\rho)$, $M^2(r)$, r_c, r_{inf}, ξ_∞, c_s^∞, frozen-amplitude radius);
- paper9_closed_form_checks.py: recomputes and compares every closed-form number in Sections 4-6 and 9 (matter-Compton closures, BPS benchmark, crossing point, window edges for $\mathcal{R}=\pi$ and 2π, energy and nucleosynthesis bounds, regime table);
- paper9_four_channel.py: the three-zone four-channel scattering calculation of Section 7.2, writing paper9_four_channel_table.csv (Table 5), paper9_four_channel_horizon_quench.csv (Table 6), paper9_four_channel_wallscan.csv, paper9_four_channel_shapes.csv, and paper9_four_channel_convergence.csv;
- paper9_four_channel_figure.py: Figure 3 from the CSV output;
- paper9_spinodal_window_scan.py: Table 7 and paper9_spinodal_window_scan.csv.

The figures of Sections 4, 6, 8, and 9 display the closed-form relations and tabulated values verified by these scripts.